

Cooperation and competition of gamma oscillation mechanisms

Atthaphon Viriyopase,^{1,2,3} Raoul-Martin Memmesheimer,^{1,3,4} and Stan Gielen^{1,2}

¹Donders Institute for Brain, Cognition and Behaviour, Radboud University Nijmegen (Medical Centre), Nijmegen, The Netherlands; ²Department for Biophysics, Faculty of Science, Radboud University Nijmegen, Nijmegen, The Netherlands;

³Department for Neuroinformatics, Faculty of Science, Radboud University Nijmegen, Nijmegen, The Netherlands; and

⁴Center for Theoretical Neuroscience, Columbia University, New York, New York

Submitted 22 May 2015; accepted in final form 23 February 2016

Viriopase A, Memmesheimer RM, Gielen S. Cooperation and competition of gamma oscillation mechanisms. *J Neurophysiol* 116: 232–251, 2016. First published February 24, 2016; doi:10.1152/jn.00493.2015.—Oscillations of neuronal activity in different frequency ranges are thought to reflect important aspects of cortical network dynamics. Here we investigate how various mechanisms that contribute to oscillations in neuronal networks may interact. We focus on networks with inhibitory, excitatory, and electrical synapses, where the subnetwork of inhibitory interneurons alone can generate interneuron gamma (ING) oscillations and the interactions between interneurons and pyramidal cells allow for pyramidal-interneuron gamma (PING) oscillations. What type of oscillation will such a network generate? We find that ING and PING oscillations compete: The mechanism generating the higher oscillation frequency “wins”; it determines the frequency of the network oscillation and suppresses the other mechanism. For type I interneurons, the network oscillation frequency is equal to or slightly above the higher of the ING and PING frequencies in corresponding reduced networks that can generate only either of them; if the interneurons belong to the type II class, it is in between. In contrast to ING and PING, oscillations mediated by gap junctions and oscillations mediated by inhibitory synapses may cooperate or compete, depending on the type (I or II) of interneurons and the strengths of the electrical and chemical synapses. We support our computer simulations by a theoretical model that allows a full theoretical analysis of the main results. Our study suggests experimental approaches to deciding to what extent oscillatory activity in networks of interacting excitatory and inhibitory neurons is dominated by ING or PING oscillations and of which class the participating interneurons are.

gamma oscillations; ING; PING; gap junction; interneuron

NEURONAL OSCILLATIONS in the gamma band (30–80 Hz) have been found in many cortical areas and have been associated to various sensory, motor, and cognitive tasks (see, e.g., Fries 2009; Schoffelen et al. 2005; Uhlhaas and Singer 2006). They have been linked to input selectivity (Börgers and Kopell 2008), reference signals for temporal encoding (Buzsáki and Chrobak 1995; Hopfield 1995), feature binding of sensory information into a coherent percept (Gray and Singer 1989), as well as storage and retrieval of information (Lisman 1999; Lisman and Idiart 1995). Numerous reviews discuss the biological processes (Gray 1994; Laurent 2002; Traub et al. 2002; Whittington et al. 2000) and the synaptic mechanisms (Bartos et al. 2007; Buzsáki and Wang 2012) underlying gamma oscillations as well as possible diseases that may be due to their malfunction (Lewis et al. 2005; Llinás et al. 1999; Spencer et al. 2003; Uhlhaas and Singer 2006). We note that although

gamma oscillations can be found in many cortical areas (Buzsáki and Draguhn 2004; Gray and Singer 1989), they have been particularly well studied in the hippocampus (Bragin et al. 1995; Buzsáki et al. 1983; Csicsvari et al. 2003) because of their prominent appearance (Forster et al. 2006) and their explicit role in exploratory behavior (Bragin et al. 1995).

The two major mechanisms that have been suggested to underlie gamma oscillations (Buzsáki and Wang 2012) are interneuronal gamma (“ING”), which is thought to be related to tonic excitation of reciprocally coupled inhibitory interneurons (Cobb et al. 1995; Friesen 1994; Lytton and Sejnowski 1991; Traub et al. 1996; Whittington et al. 1995, 2000), and pyramidal-interneuron gamma (“PING”), which is mediated by coupled populations of excitatory pyramidal cells and inhibitory interneurons (Börgers and Kopell 2003; Tiesinga et al. 2001; Whittington et al. 2000). Gamma oscillations generated by different mechanisms may serve different biological functions. In the present article we therefore investigate which mechanism will dominate the dynamics of a network that could in principle generate oscillations according to different mechanisms and how the dominant mechanism may switch.

The coupling between interneurons, which yields synchronized oscillations of interneuronal networks in the gamma frequency range (Bartos et al. 2002, 2007; Kopell and Ermentrout 2004; McBain and Fisahn 2001; Tamas et al. 2000; Whittington et al. 2000), includes both synaptic coupling and gap junctions. Both theoretical and experimental studies have shown that inhibitory synapses alone may be sufficient for generating gamma oscillations (e.g., Bartos et al. 2007; van Vreeswijk et al. 1994). However, gap junctions are sometimes required (Deans et al. 2001; Hormuzdi et al. 2001; Kopell and Ermentrout 2004) and may also induce oscillations in the absence of chemical synapses (Gibson et al. 1999; Kopell and Ermentrout 2004; Mann-Metzer and Yarom 1999). Some studies reported that gap junctions impede synchrony of neuronal activity (Bou-Flores and Berger 2001; Pfeuty et al. 2003). Since both gap junctions and chemical synapses are abundant in many brain areas (Fukuda and Kosaka 2000; Galarreta and Hestrin 2002), they should both be taken into account in order to understand ING. Gap junctions and inhibitory synapses between interneurons may be supportive or hindering, as they may contribute to both in-phase and antiphase oscillations (Bem et al. 2005; Bem and Rinzel 2004; Long et al. 2002; Pfeuty et al. 2005). When GABA-mediated inhibition is strong, addition of a small electrical conductance can increase the degree of synchronization more than a larger increase in inhibitory conductance (Kopell and Ermentrout 2004; White et al. 1998a).

Address for reprint requests and other correspondence: R.-M. Memmesheimer, Center for Theoretical Neuroscience, Columbia Univ., Kolb Research Annex, 1051 Riverside Dr., New York, NY 10032-2695 (e-mail: rm3354@cumc.columbia.edu).

The above studies indicate that the impact of electrical and chemical synapses on oscillatory activity is complicated and can depend on the details of the network setup and the type of oscillation. This motivated us to investigate this impact on the ING and PING oscillations in networks that are modeled according to neurobiological knowledge on hippocampal networks.

Most theoretical studies on ING rhythms have investigated oscillations in networks of interneurons with a tonic excitatory drive to the interneurons without reciprocal connections with pyramidal cells and without the input from these pyramidal cells to the interneurons. In contrast, theoretical studies on PING oscillations have mainly investigated networks with external input to pyramidal cells, which are reciprocally coupled to interneurons that do not fire on their own; thus the drive to the interneurons in these PING rhythms is weak. ING oscillations with only external input to interneurons on the one hand, and PING oscillations with a strong drive to pyramidal cells and weak input to interneurons on the other hand, are presumably two extremes of more common situations with variable amounts of comparable input to both interneurons and pyramidal cells. We name these two extremes “pure” ING and “pure” PING and use them as reference to study how ING and PING interact in networks that could in principle generate both kinds of rhythms.

In vitro studies have addressed this topic by adding drugs that modify the excitability of pyramidal cells or interneurons or that modify the synaptic interactions between pyramidal cells and interneurons (see, e.g., Fisahn et al. 1998, 2004; Gloveli et al. 2005; Hajos et al. 2004; Palhalmi et al. 2004). Theoretical analyses of interactions between ING and PING rhythms are scarce. Börgers and Kopell (2003, 2005) and Börgers and Walker (2013) studied transitions from PING to irregular oscillations (e.g., the “walkthrough transition”), to asynchronous activity with or without suppressed E cells (with suppressed E cells: “suppression transition”), and to ING oscillations with suppressed E cells as another variant of the suppression transition. Most closely related to our work, Börgers and Walker (2013) studied different forms of the suppression transition, from PING to asynchronous or oscillatory activity, both with suppressed E cells.

We study the transition from PING to ING with active E cells for networks with type I interneurons and type II interneurons: For type I interneurons an excitatory input always advances their spiking, while the same input arriving soon after spiking of type II interneurons delays their next spiking (see Hansel et al. 1995 for this definition of type I and type II neurons). Considering both types of interneurons allows us on one hand to make contact with the many network oscillation studies that have used type I interneurons. On the other hand, it accounts for the literature that suggests that interneurons relevant for gamma oscillations often belong to the class of type II neurons (see Erisir et al. 1999; Tateno et al. 2004; Tateno and Robinson 2007; Tikidji-Hamburyan et al. 2015). Furthermore, it allows us to draw conclusions on the robustness of the observed effects.

The transition between PING and ING with active pyramidal cells as considered in our study may be a biologically highly relevant one: It may allow switching between rhythms of neuronal activity related to different cognitive functions, keeping the pyramidal cells active, which are able to provide

information transfer to more distant brain areas through their long-range connectivity. Indeed, excitatory neurons are experimentally found to be active during ING oscillations (e.g., Cardin et al. 2009; Sohal et al. 2009; Whittington et al. 2011).

As a first step toward understanding the behavior of a full network where ING and PING rhythms interact, we analyze the properties of pure ING in a reduced network that cannot generate PING and pure PING oscillations in a reduced network that cannot generate ING. To make the model biologically plausible and to facilitate experimental validation of our results, we have modeled a network of the hippocampal region CA1 using data and biologically plausible parameter values from the literature. We use CA1 as a paradigmatic region where different kinds of gamma oscillations can be generated, at least *in vitro* (Bartos et al. 2007). By eliminating the projections from the pyramidal cells to the interneurons, we create networks only generating ING oscillations (pure ING). By removing the external input to the interneurons, we create networks only allowing for PING (pure PING). With the complete model, including projections from pyramidal cells and with a constant drive to the interneurons, we investigate the interactions between ING and PING oscillations. To explain the results of the extensive computer simulations, we present a theoretical model that allows for a full theoretical analysis of the stable states of network oscillations when ING and PING interact. This model qualitatively reproduces and explains the results of the computer simulations.

METHODS

Single-Compartment Hodgkin-Huxley-Type Model

In our computer simulations we use a single-compartment Hodgkin-Huxley-type model for CA1 pyramidal (E) cells as suggested in Nowacki et al. (2011), with transient I_{Na_T} and persistent I_{Na_P} Na^+ currents, T-type I_{Ca_T} and high-voltage-activated $I_{\text{Ca}_{\text{H}}}$ Ca^{2+} currents, a delayed rectifier $I_{\text{K}_{\text{DR}}}$, an M-type K^+ current I_{K_M} , and a leak current I_L . The free dynamics of the membrane potential obeys the differential equation $C_{m,E} \frac{dV}{dt} = -I_{\text{Na}_T} - I_{\text{Na}_P} - I_{\text{Ca}_T} - I_{\text{Ca}_{\text{H}}} - I_{\text{K}_{\text{DR}}} - I_{\text{K}_M} - I_L$, with the membrane capacitance $C_{m,E}$. The seven ionic currents follow $I_x = g_x m_x^M h_x^N (V - E_x)$, where x stands for Na_T , Na_P , Ca_T , Ca_{H} , K_{DR} , K_M , or L with different nonnegative integer exponents M and N ; g_x stands for the maximal conductance, m_x for the activation gating variable, h_x for the inactivation gating variable, and E_x for the reversal potential. The parameters for the CA1 pyramidal cell model in Nowacki et al. (2011) yield a passive time constant $\tau_{0,E} = C_{m,E}/g_L \approx 50$ ms. Note that $g_{\text{Ca}_{\text{H}}}$ in Table 2 of Nowacki et al. 2011 should be 2.6 mS/cm^2 instead of the value 0.74 mS/cm^2 , which was used in that report.

We model the fast-spiking interneurons (I cells) in CA1 hippocampus either as type I neurons, where excitatory input always gives a phase advance of the neuronal oscillator (see Krogh-Madsen et al. 2012), or as type II neurons, where excitatory input in the early phase of the firing cycle causes a phase delay and a phase advance in later phases of the firing cycle (Ermentrout 1996; Izhikevich 2007). For the networks with type I interneurons we use Wang-Buzsáki (WB) neurons (Wang and Buzsáki 1996). These WB neurons have a transient Na^+ current (I_{Na_T}), a delayed-rectifier K^+ current ($I_{\text{K}_{\text{DR}}}$), and leak (I_L). The differential equation describing the membrane potential is given by $C_{m,I} \frac{dV}{dt} = -I_{\text{Na}_T} - I_{\text{K}_{\text{DR}}} - I_L$. Figure 1 shows the voltage trace as a function of time, the firing rate as a function of the input current, and the phase-response curve (PRC). We display the standard infinitesimal PRC, i.e., the phase lead or phase lag in response to an infinitesimal positive instantaneous input, normalized

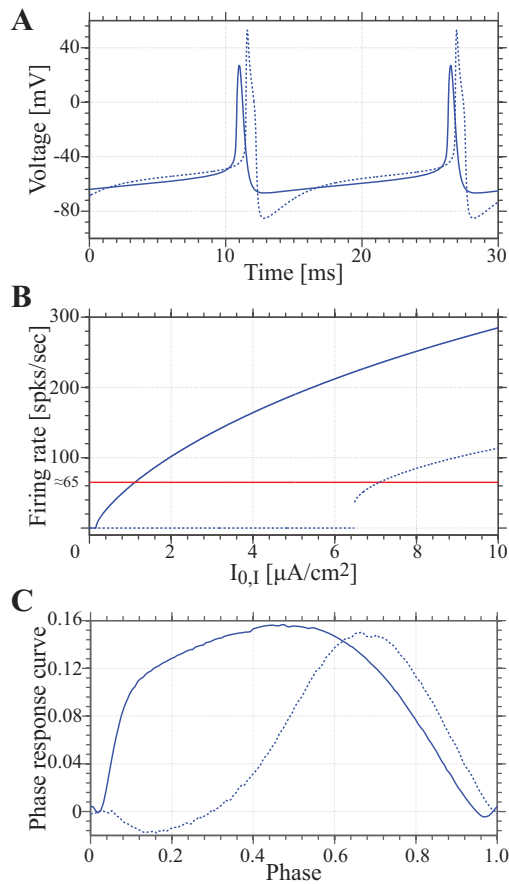


Fig. 1. Dynamics of the Wang-Buzsáki and Börgers-Walker interneurons. *A*: example of voltage traces of the Wang-Buzsáki (solid line) and Börgers-Walker (dashed line) interneurons for $I_{0,1} = 1.1 \mu\text{A}/\text{cm}^2$ for the Wang-Buzsáki interneuron and $I_{0,1} = 7.1 \mu\text{A}/\text{cm}^2$ for the Börgers-Walker interneuron. *B*: firing rate vs. the external current for the Wang-Buzsáki (solid line) and Börgers-Walker (dashed line) interneurons. *C*: infinitesimal phase-response curves of the Wang-Buzsáki (solid line) and Börgers-Walker (dashed line) interneurons are of type I and type II, respectively.

by the input strength, as a function of the phase in the cycle. We adopt the standard parameter values suggested in Wang and Buzsáki (1996). With these parameter values, the time constant $\tau_{0,1} = C_{m,1}/g_{L,1}$ equals 10 ms.

For the interneuron network with type II neurons, we use the Hodgkin-Huxley-type model proposed by Erisir et al. (1999), but modified as described by Börgers and Walker (2013). We refer to this neuron model as the Börgers-Walker neuron. Figure 1 shows the voltage trace as a function of time, the firing rate as a function of the input current, and the PRC for this neuron. In early stages of the firing cycle, the PRC has negative values, corresponding to a phase delay, which is typical for type II neurons. With the standard parameter values given in Börgers and Walker (2013), the passive time constant of this interneuron model is 2 ms. To facilitate a comparison of the results for both types of interneurons, the mean external input current was adjusted in our simulations to produce the same intrinsic firing frequency for the network of inhibitory type I and type II interneurons (i.e., an input near $1 \mu\text{A}/\text{cm}^2$ for the WB neuron and near $7 \mu\text{A}/\text{cm}^2$ for the Börgers-Walker neuron to produce oscillations near 65 Hz; see Fig. 1*B*).

E and I cells are connected by AMPA synapses ($E \rightarrow E$ and $E \rightarrow I$), GABA_A synapses ($I \rightarrow E$ and $I \rightarrow I$), and gap junctions ($I \rightarrow I$). The synaptic input by the AMPA and GABA_A-receptor-mediated synapses for cell i are modeled by $-gs_i(t - t_k - \tau_l)(V_i - E_{\text{rev}})$, where g , s_i , t_k , τ_l , and E_{rev} are the synaptic conductance, the

time course of the conductance, the time of the k th presynaptic action potential, latency, and the reversal potential. For AMPA synapses, $E_{\text{rev}} = 0 \text{ mV}$ (Cutsuridis et al. 2010) with $g = g_{E \rightarrow I}$ or $g = g_{E \rightarrow E}$. For GABA_A synapses $E_{\text{rev}} = -75 \text{ mV}$ (Cutsuridis et al. 2010) with $g = g_{I \rightarrow I}$ or $g = g_{I \rightarrow E}$. The time course of the conductance s_i is modeled by the normalized difference between two exponential functions (Gerstner and Kistler 2002) with rise time τ_r and decay time τ_d . For $E \rightarrow E$ connections, $\tau_l = 2.5 \text{ ms}$ (see Debanne et al. 1995), $\tau_r = 0.5 \text{ ms}$, and $\tau_d = 2.5 \text{ ms}$ with a peak conductance of 2.3 nS (see Memmesheimer 2010 and references therein for this and subsequent peak conductances). For $E \rightarrow I$ connections the parameter values are $\tau_l = 1.3 \text{ ms}$, $\tau_r = 0.45 \text{ ms}$, and $\tau_d = 1.0 \text{ ms}$ (Brunel and Wang 2003; Geiger et al. 1997) with a peak conductance of 3.2 nS . For $I \rightarrow E$, $\tau_l = 0.95 \text{ ms}$, $\tau_r = 0.25 \text{ ms}$, and $\tau_d = 4.0 \text{ ms}$ (Bartos et al. 2002) with a peak conductance of 5 nS . For $I \rightarrow I$, $\tau_l = 0.6 \text{ ms}$, $\tau_r = 0.3 \text{ ms}$, and $\tau_d = 2.0 \text{ ms}$ (Bartos et al. 2002) with a peak conductance of 4 nS . Hence, with a typical total surface area of $21,590 \mu\text{m}^2$ for a CA1 pyramidal cell (Routh et al. 2009) and $18,069 \mu\text{m}^2$ for a CA1 basket cell (Cutsuridis et al. 2010), $g_{E \rightarrow E} = 0.04 \text{ mS}/\text{cm}^2$, $g_{E \rightarrow I} = 0.034 \text{ mS}/\text{cm}^2$, $g_{I \rightarrow E} = 0.11 \text{ mS}/\text{cm}^2$, and $g_{I \rightarrow I} = 0.062 \text{ mS}/\text{cm}^2$. The gap junctions between I cells are modeled by $-g(V_i - V_j)$ with conductance $g_{GJ} = 0.01 \text{ mS}/\text{cm}^2$ (Bartos et al. 2002).

We assume a ratio of excitatory and inhibitory neurons $N_E/N_I = 4$ with 5,000 neurons in total. Synaptic connectivity is random and sparse. We adopt connection probabilities reported for the CA1 region (Ascoli and Atkeson 2005), $E \rightarrow E$: 0.0067, $E \rightarrow I$: 0.3, $I \rightarrow E$: 0.67, and $I \rightarrow I$: 0.3. I cells are connected by gap junctions with probability 0.004 (Bartos et al. 2002). See DISCUSSION for a careful interpretation of these choices.

E cells receive external currents $I_{\text{app},E} = I_{0,E} + \sigma_E(C_{m,E}/\sqrt{\tau_{0,E}})\xi(t)$, where $I_{0,E}$ is the mean excitatory current, ξ is independent Gaussian white noise (zero mean, unit variance), and $C_{m,E}$ denotes the membrane capacitance, $\tau_{0,E}$ the passive time constant, and σ_E the standard deviation of stochastic fluctuations. Similarly, I cells receive external inputs $I_{\text{app},I} = I_{0,I} + \sigma_I(C_{m,I}/\sqrt{\tau_{0,I}})\xi(t)$.

We solve the differential equations for the membrane potential of the E and I cells using the Euler-Maruyama method with $\Delta t = 0.01 \text{ ms}$ (Goldwyn and Shea-Brown 2011), well below all relevant timescales in the model. At the start of each simulation, neurons that are driven above their spiking threshold are initialized at a uniformly drawn random point on their firing limit cycle; the remaining neurons are initialized at their resting state. After a time interval of 500 ms (to eliminate the effect of initial network conditions), we collect firing activities of the E and I cells in the time interval from 500 to 2,000 ms to calculate the oscillation frequency of the network, the mean firing rates, and the coherence κ among cell activity as defined in Wang and Buzsáki (1996). To estimate κ , we average the pairwise coherences (cf. Eq. 2.5 of Wang and Buzsáki 1996) between all neurons in a randomly chosen set of 100 neurons. In our study, dynamics with $\kappa > 0.08$ are classified as showing a rhythm. To calculate the oscillation frequency, the firing activities of the E and I cells are used to construct the corresponding population activity with a 1-ms time resolution (see Gerstner and Kistler 2002). Next we remove the nonzero DC average of the population activity by subtracting the mean population activity. The power spectral density of the resulting population activity is calculated with Welch's method (Welch 1967) with 50% overlapping. The power spectral density is then normalized in order to have unit energy in the frequency domain. The frequency of the oscillation is determined as the frequency corresponding to the peak power in the power spectral density. All results, except for the spike raster diagrams, are averaged over 10 independent runs.

Phase Model

To substantiate the results based on the single-compartment Hodgkin-Huxley-type models, we investigate the dynamics of a pair of interacting simplified E and I cells representing the dynamics of synchronized E and I neuron populations, respectively. The model allows a full analytical solution. For this simple model we assume two pulse-coupled neurons: an excitatory (E) neuron with excitatory projection $\varepsilon_{E \rightarrow I}$ to an inhibitory (I) neuron, which reciprocally inhibits the E neuron with coupling strength $\varepsilon_{I \rightarrow E}$. Since the I neuron represents the synchronous activity of a population of coupled inhibitory neurons, it has self-inhibitory coupling $\varepsilon_{I \rightarrow I}$. All couplings have a delay τ . The synapses are assumed to be instantaneous, in the sense that the membrane potential is incremented by an amount ε when the input arrives τ after the spike generation in the presynaptic neuron.

We use a phase representation, where $\varphi_E(t)$ and $\varphi_I(t)$ represent the phases of the E and I neurons at time t . Without input, the phases increase linearly as $d\varphi_E(t)/dt = d\varphi_I(t)/dt = 1$ until they reach the phase thresholds Θ_E and Θ_I and are reset to zero. We analyze the stable states of 1:1 phase-locked firing for the case where the E neuron and the I neuron are represented by leaky integrate-and-fire (LIF) neurons (*model 1*) and for the case where the I neuron is a so-called sine neuron (*model 2*), which is a paradigmatic neuron of type II (Brown et al. 2004; Ermentrout et al. 2001; Hansel et al. 1995; Izhikevich 2007).

Model 1. In *model 1* the E and I neurons are both LIF neurons. The dynamics of the membrane potential V_{LIF} are given by

$$\frac{dV_{LIF}(t)}{dt} = -\gamma V_{LIF}(t) + I(t), \quad (1)$$

where we use the standard form for the dynamics of the LIF neuron (Gerstner and Kistler 2002), γ is equal to $1/\sigma$, with the time constant of the LIF neuron σ . For simplicity, we assume that γ is the same for the E and I neurons; without loss of generality its value is set to 1. Additionally, we assume that when V_{LIF} of a neuron reaches a voltage threshold defined to be 1, the neuron sends a spike, which arrives after a time delay τ . When the voltage reaches the voltage threshold, it is instantaneously reset to 0. The voltage threshold corresponds to the phase thresholds (and free periods) Θ_E of the E neuron and Θ_I of the I neuron where $V_{LIF,E}(\Theta_E) = V_{LIF,I}(\Theta_I) = 1$. The external current applied to the E and I neurons is then $1/(1 - e^{-\Theta})$, with Θ referring to Θ_E or Θ_I for the E or I neuron, respectively. The LIF neuron represented by *Eq. 1* is a type I neuron, and an analytical expression for its PRC can be found in the literature (Canavier et al. 2013; Izhikevich 2007; Lewis and Rinzel 2003; van Vreeswijk et al. 1994).

The transfer function $H_{LIF}(\varphi; \Theta, \varepsilon)$, which gives the new phase of the LIF neuron after arrival of a spike at the synapse with coupling strength ε when the phase of the LIF neuron is $\varphi \leq \Theta$, is given by

$$H_{LIF}(\varphi; \Theta, \varepsilon) = \begin{cases} -\ln[e^{-\varphi} - \Gamma_{LIF}(\Theta, \varepsilon)] & \text{for } V_{LIF}(\varphi) + \varepsilon < 1 \\ 0 & \text{otherwise,} \end{cases} \quad (2)$$

where $\Gamma_{LIF}(\Theta, \varepsilon) = (1 - e^{-\Theta})\varepsilon$.

In *Eq. 1*, $I(t)$ represents the time-dependent total input to the neuron. This implies that for pure ING oscillations, the input $I(t)$ to an interneuron gathers the external input (which is constant in our simulations) plus the time-dependent inhibitory input from the other inhibitory neurons in the network, represented by the self-inhibition after firing. For pure PING, the input to the E neuron gathers the external (constant) input to the E neuron plus the time-dependent inhibitory input from the interneuron.

Model 2. Motivated by experimental findings suggesting that interneurons relevant for typical gamma oscillations belong to the category of type II neurons, we also performed phase analysis for the case where the E neuron is represented by a LIF neuron and the I

neuron by a sine neuron, i.e., a neuron that has an infinitesimal PRC (iPRC) given by

$$\text{iPRC}_{\text{sine}}(\varphi; \Theta) = -\sin\left(\frac{2\pi}{\Theta}\varphi\right) \quad (3)$$

(cf., e.g., Goel and Ermentrout 2002; Winfree 1967). Note that the neuron belongs to the category of type II neurons: The iPRC in *Eq. 3* is negative in the first half of the cycle, such that a positive input generates a phase delay when $0 < \varphi < \Theta/2$, and it is positive for the second half of the cycle, i.e., a positive input generates a phase advance when $\Theta/2 < \varphi < \Theta$. The iPRC does not fully specify the neural dynamics as it only determines the derivative of the transfer function at $\varepsilon = 0$,

$$\frac{\partial H_{\text{sine}}(\varphi; \Theta, \varepsilon)}{\partial \varepsilon} \Big|_{\varepsilon=0} = \text{iPRC}_{\text{sine}}(\varphi; \Theta) \quad (4)$$

We characterize the transfer function by the requirement that the response of the neuron to a large input equals the linear summation of responses of the neuron to a number of small inputs that arrive separately within a short time interval. This leads to the defining differential equation

$$\frac{\partial H_{\text{sine}}(\varphi; \Theta, \varepsilon)}{\partial \varepsilon} = \text{iPRC}_{\text{sine}}(H_{\text{sine}}(\varphi; \Theta, \varepsilon); \Theta) \quad (5)$$

Note that for $\varepsilon = 0$ *Eq. 5* reduces to *Eq. 4* since $H_{\text{sine}}(\varphi; \Theta, 0) = \varphi$. The explicit expression for $H_{\text{sine}}(\varphi; \Theta, \varepsilon)$ and the analytical expressions for the firing frequencies in various conditions can be found in the APPENDIX. Further details and the derivations will be given in a separate article.

RESULTS

Role of Gap Junctions and Chemical Synapses in ING Oscillations

How do gap-junctional coupling and recurrent chemical connectivity interact to give rise to synchronous oscillations in our networks? To address this question we focus on the interneuron networks, which possess electrical coupling, and on the resulting ING oscillations. We reduce the topology of the network described in METHODS by eliminating the projections from the excitatory pyramidal cell population (E cells) to the I cells (Fig. 2A). This prevents the network from generating PING oscillations.

We first study the ING oscillations in a network of WB type I neurons. Depending on the strengths of chemically synaptic and gap-junctional coupling, the network of I cells may or may not reveal oscillatory activity. The overall picture is shown in Fig. 2. When recurrent inhibition $g_{I \rightarrow I}$ is very small, there is no or only weak synchronization in the I cells (Fig. 2B, *a* and *b*) depending on the strength of the gap-junctional coupling, which is in agreement with previous findings (Abbott and van Vreeswijk 1993; Bem and Rinzel 2004; Brunel and Hakim 1999; Chow and Kopell 2000; Traub et al. 2001; Wang and Rinzel 1992). This is because in order to create ING, interneurons require a certain minimal amount of inhibition from other interneurons (Wang and Buzsáki 1996). When $g_{I \rightarrow I}$ increases, e.g., from *b* to *c* in Fig. 2B, firing becomes more synchronous and the firing rate decreases because of the increasing amount of inhibition (Fig. 2B*c*) (see Kopell and Ermentrout 2004). The mean firing rate and the coherence between firing of I cells are shown in Fig. 2C, *left* and *right*, respectively. We note that the

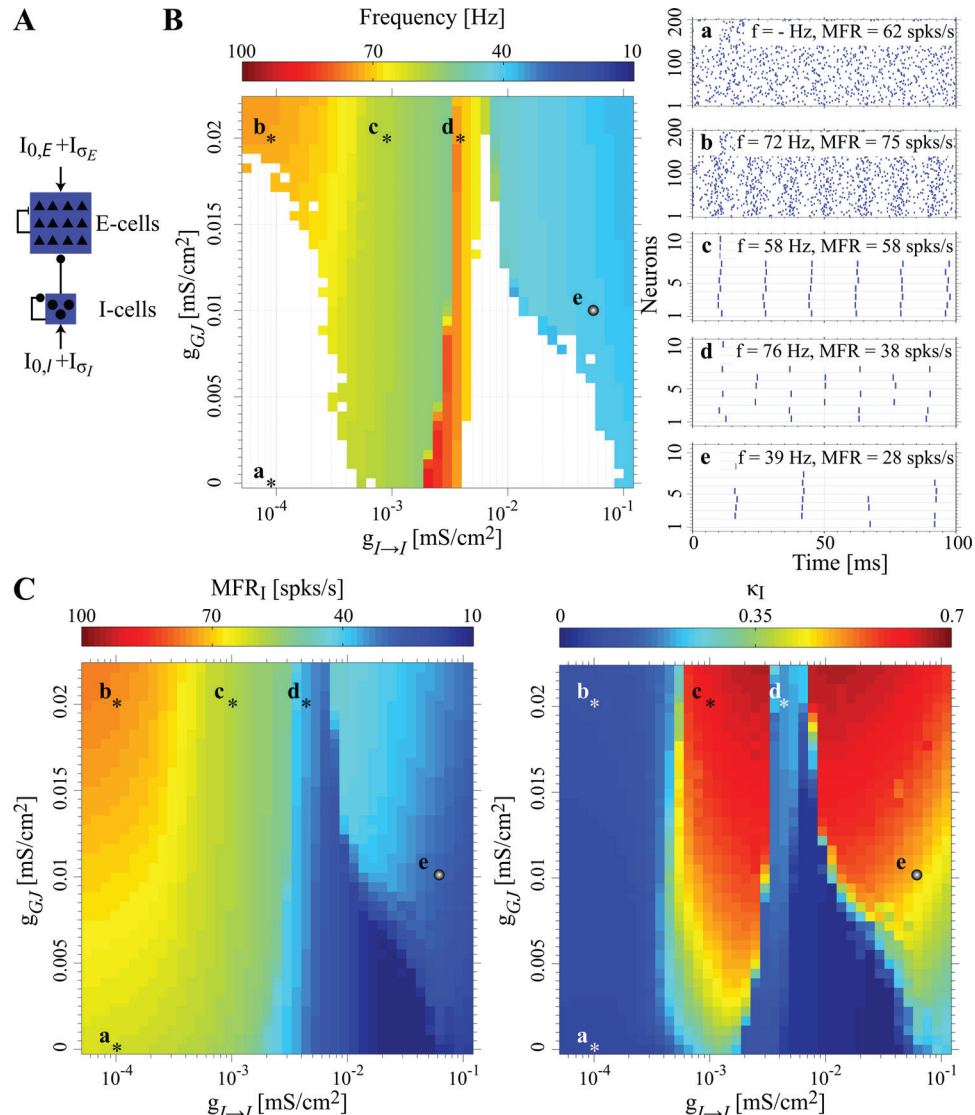


Fig. 2. ING oscillations for a reduced network with type I interneurons coupled by inhibitory synapses and gap junctions. **A:** schematic overview of the network with reduced topology to focus on ING oscillations. E cells receive inhibitory inputs from I cells, but connections from E cells to I cells are removed. **B:** oscillation frequency in the network of interneurons for various gap-junctional (g_{GJ}) and synaptic ($g_{I \rightarrow I}$) strengths. *a–e*: Raster plots illustrating the different modes of firing corresponding to the combinations of $g_{I \rightarrow I}$ and g_{GJ} . *a*: No oscillation. *b*: Weak gamma-range oscillations generated by gap junctions. *c–e*: Strongly synchronous ING-based oscillations where neurons spike once per cycle (*c*), alternatingly (*d*), and in changing synchronously firing groups (*e*). Parameter values corresponding to the spiking activities (*a–e*) are highlighted in the main panel in **B** by asterisks and gray sphere. White area corresponds to parameter values where significant oscillatory activity was absent (METHODS). Gray sphere marked *e* indicates the parameter values found in experiments in the CA1 region. Parameter values: $I_{0,I} = 1.1 \mu\text{A}/\text{cm}^2$, $\sigma_I = 0.5 \text{ mV}$. **B**, *a–e*: $(g_{I \rightarrow I}, g_{GJ}) = (10^{-4}, 0)$, $(10^{-4}, 0.02)$, $(10^{-3}, 0.02)$, $(3.6 \times 10^{-3}, 0.02)$, and $(0.062, 0.01) \text{ mS}/\text{cm}^2$. **C**: mean firing rate of the interneurons (left) and the coherence of firing (right).

coarse scaling of the coherence in Fig. 2C, right, obscures a gradual increase in coherence for increasing values of gap junction coupling for small values of $g_{I \rightarrow I}$. An increase of $g_{I \rightarrow I}$ from *c* to *d* in Fig. 2B first decreases the oscillation frequency. However, at some point a transition occurs to a higher frequency of the ING network oscillations. This higher oscillation frequency co-occurs with a lower mean firing rate of the I cells, which can be explained by alternating firing of two clusters into which the I neuron population has dissociated (Fig. 2Bd and point *d* in Fig. 2C). We note that such a state may be biologically irrelevant since it is sensitive to heterogeneity in the external currents to the neurons. Increasing $g_{I \rightarrow I}$ even further at the same value of the gap-junctional coupling (for g_{GJ} below $\sim 0.02 \text{ mS}/\text{cm}^2$) yields asynchrony (see Fig. 2B).

Stronger gap junction coupling seems to counteract the desynchronization such that the transition from the high oscillation ING synchrony to asynchrony occurs at larger values of $g_{I \rightarrow I}$. Interestingly, we find that when the strength of the chemical synapses increases further, ING reappears. Experimentally found values (see METHODS) for chemically synaptic coupling and gap junction strengths are illustrated by the letter “*e*” in Fig. 2B.

Figure 3 shows the results for ING oscillations when the type I WB neuron is replaced by the type II Börgers-Walker neuron. One of the characteristics of type II neurons is that the frequency-current relation is discontinuous; if the neuron starts firing, it will do so with a firing rate significantly above zero (see Fig. 1B). Moreover, type II neurons have a

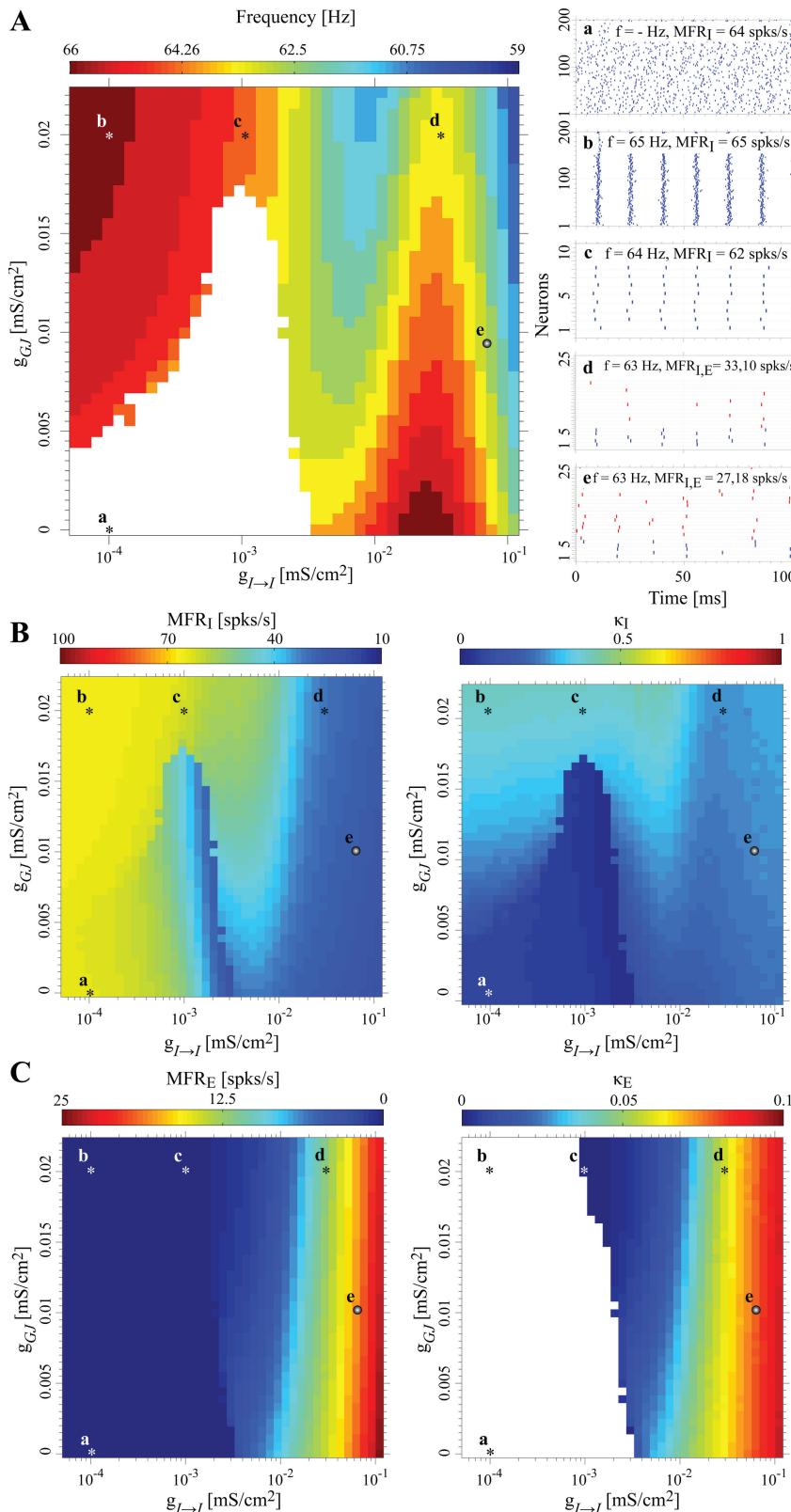


Fig. 3. ING oscillations for a reduced network with type II interneurons coupled by inhibitory synapses and gap junctions. Network topology is as in Fig. 2A. *A*: frequency of network oscillation vs. gap-junctional (g_{GJ}) and synaptic ($g_{I \rightarrow I}$) strengths. *a–e*: Raster plots illustrating the different modes of firing in *A*. *a*: No oscillations. *b*: Gamma-range oscillations generated by gap junctions. *c*: Strongly synchronous ING-based oscillations. *d* and *e*: In changing synchronously firing groups. Red vertical bars display spiking of pyramidal neurons; blue vertical bars display spiking of interneurons. In some parts of the parameter space, the E cells do not fire (as in *a*) or fire at a low rate (as in *b* and *c*; spiking not shown because of low rate). *B* and *C*: coherence of firing in the network of interneurons (right) and the mean firing rate (left) of the interneurons (*B*) and the pyramidal cells (*C*). Parameter values: $I_{0,I} = 7.1 \mu\text{A}/\text{cm}^2$, $\sigma_I = 0.5 \text{ mV}$, $I_{0,E} = 5.8 \mu\text{A}/\text{cm}^2$, $\sigma_E = 60 \text{ mV}$. *A*, *a–e*: $(g_{I \rightarrow I}, g_{GJ}) = (10^{-4}, 0), (10^{-4}, 0.02), (10^{-3}, 0.02), (3 \times 10^{-2}, 0.02)$, and $(0.062, 0.01) \text{ mS}/\text{cm}^2$.

PRC with a phase delay for excitatory input arriving shortly after firing (Fig. 1C) and, which is equivalent, a phase advance for inhibitory inputs after firing. The phase advance accelerates the neuron in its cycle, reducing the interval to the next spike. This mechanism explains why the network

and thus individual neuron firing frequencies for type II neurons in Fig. 3A do not decrease as much as for type I neurons (see Fig. 2B) when $g_{I \rightarrow I}$ increases. (Note that the color code for ING oscillation frequency is different in Fig. 2B and Fig. 3A).

As for the type I neurons, the firing frequency of oscillations in the network of interneurons (Fig. 3A) and the coherence of synchronous firing in the ING network increases (Fig. 3B, right, and Fig. 3A, *a* and *b*) when the gap-junctional coupling strength increases for small values of $g_{I \rightarrow I}$. Qualitatively similar to Fig. 2, increasing $g_{I \rightarrow I}$ at a constant value of the gap-junctional coupling gives rise to a decrease of the firing frequency in the network of interneurons (see Fig. 3A, *b* and *c*). As already mentioned, this decrease is much smaller than for type I neurons, since inhibitory input after firing of the interneuron gives rise to a phase advance or a phase delay for type II neurons, rather than only a phase delay as for type I neurons. Furthermore, we find that the increase of weak synaptic coupling has a desynchronizing effect on the synchronization by gap junctions: Synchronization disappears when weak synaptic coupling becomes stronger (transition into the white region in Fig. 3A, bottom left). In the region of parameter space where the gap-junctional coupling is not strong enough to maintain synchronization for all values of $g_{I \rightarrow I}$ (for g_{GJ} below ~ 0.017 mS/cm²), the network synchronizes again as $g_{I \rightarrow I}$ increases further to higher values. The region without synchronization can be related to a region with coexistence of stable in-phase and antiphase synchronization in simulations of two-neuron systems with inhibitory and gap junction coupling (cf. Bem and Rinzel 2004 for the general setup), where the parameters are adapted to match those of our large networks. When the value of $g_{I \rightarrow I}$ is at $\sim 10^{-3}$ mS/cm² (*condition c*), a further increase (e.g., from *c* to *d* in Fig. 3A) gives rise to a decrease of the oscillation frequency of the ING network followed by an increase (see Fig. 3A). The decrease in ING frequency and mean firing rate of I cells (see Fig. 3, A and B) for increasing (small, *b* to *c*) values of $g_{I \rightarrow I}$ is due to the increasing inhibitory input for larger values of $g_{I \rightarrow I}$. When $g_{I \rightarrow I}$ increases to larger values, the stable mode of firing of the network changes from in-phase to antiphase. This is in agreement with previous results in two-neuron systems by Bem and Rinzel (2004) and with our own simulations of two-neuron systems with parameters adapted to match those of our large networks. The change of mode leads to an increase in network oscillation frequency. In contrast to the case of type I neurons (see Fig. 2B with $g_{I \rightarrow I}$ values in the range between $\sim 6 \times 10^{-3}$ mS/cm² and 10^{-1} mS/cm²), the border between the white region of asynchrony and the colored regions of synchronized firing is largely independent of the gap junction strength (see Fig. 3A for $g_{I \rightarrow I}$ values between $\sim 10^{-3}$ mS/cm² and 3×10^{-3} mS/cm²), indicating that gap junctions do not play a major role for it. This may be dependent on the chosen parameters, e.g., gap junctions may be more supportive when introducing heterogeneity in the constant inputs to the neurons. For the type I WB neurons in Fig. 2 the transition to a higher firing frequency of the network is abrupt because of a sudden change to alternating firing of the I neurons, i.e., the type I interneurons spike once per two oscillatory cycles, causing a discrepancy between network oscillations and mean firing rate of the I cells. For the type II Hodgkin-Huxley-type neurons in Fig. 3 this transition is gradual, since type II interneurons do not switch to a mode of alternating firing, although firing gets sparser. In contrast to the network with type I interneurons, we do not find a region of desynchronization for strong inhibitory synapses.

The set of parameter values that correspond to data from the experimental literature about CA1 (*condition e* in Fig. 3A)

reveals coherent, synchronous spiking of variable subgroups of the I cells. Figure 3C, *left*, shows the mean firing rate of the E cells. In the present setup generating pure ING oscillations, there is no projection from the E cells to the interneurons (see Fig. 2A) and the E cells receive a constant external input, in addition to the inhibitory input from the network of interneurons. The coherence (Fig. 3C, right) and the mean firing rate of the E cells (Fig. 3C, *left*) increase with increasing values of $g_{I \rightarrow I}$. Because of the inhibition by the I cells, E cells fire before or near the firing of the I cells but not thereafter (Fig. 3A, *d* and *e*): The pure ING oscillations illustrate that the observation that the peak of spiking of the E cells precedes that of the I cells should not be interpreted as evidence for PING. When $g_{I \rightarrow I}$ increases, the mean firing rate of the I cells decreases because of the temporal extension and shape of the postsynaptic currents, which leads to more delay than advance despite the type II PRC (Fig. 3B, *left*). When the mean firing rate of the I cells decreases, the inhibitory input to the E cells decreases as well, which explains the higher mean firing rate of the E cells for larger values of $g_{I \rightarrow I}$ in Fig. 3C, *left*.

PING Rhythms and Firing Rate of E Cells

In our ING simulations we found that E cells can spike at a low firing rate during rhythmic activity in the I cells (see, in particular, Fig. 3Ae and Fig. 3C, *left*), in agreement with experimental findings (Fisahn et al. 1998). In contrast, for PING oscillations in typical neural network models the firing rates are often implausibly high, reaching the network oscillation rate. We now explore for our networks how excitatory neurons may spike during PING oscillations at a rate that is much lower than the network oscillation rate, even for highly synchronized PING rhythms. To focus on PING rhythms, we remove the constant input to the interneurons (Fig. 4A), which disables ING-related oscillations.

Börgers and Kopell (2003) have shown that the PING mechanism can yield perfect synchronization if the $E \rightarrow I$ synapses are sufficiently strong. In agreement with their results, our network gives almost perfect synchronization (not shown) for the biologically plausible values for $E \rightarrow I$ synapses near $g_{E \rightarrow I} = 0.034$ mS/cm² (see METHODS) without noise input to the E and I cells. In this regime, the firing rates of E and I cells agree with the frequency of the network oscillations (defined as the oscillation frequency of the population of E cells) both for type I interneurons and for type II interneurons. However, observations in both *in vivo* (Csicsvari et al. 2003) and *in vitro* (Gloveli et al. 2005) studies have shown that the firing rate of E cells is much lower than that of I cells during gamma oscillations. Orienting at the work of Börgers and Kopell (2005) and Economo and White (2012) (who investigated the effect of noise on PING rhythms) and the work of White et al. (1998b) (who proposed a role for channel noise in shaping interspike interval distributions of the pyramidal cells), we check this and investigate how our simpler Gaussian white noise input to the E cells reduces the E cell firing rate in both networks with type I and type II interneurons while still allowing for strongly synchronous PING oscillations.

For this we investigate the frequency of PING rhythms and the corresponding mean firing rates of the E and I cells as a function of the mean current $I_{0,E}$ and the noise amplitude σ_E . When $I_{0,E}$ and σ_E are too small, the network fails to generate

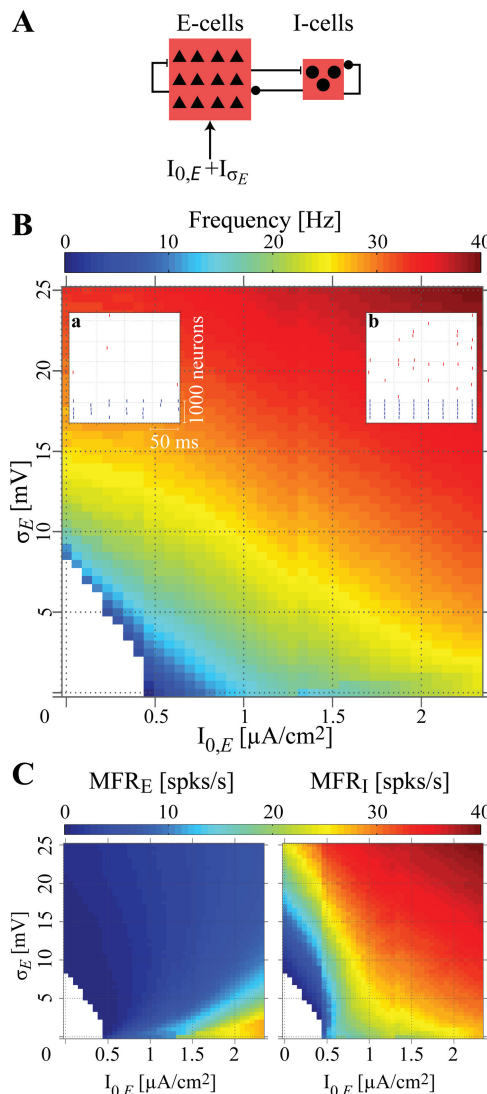


Fig. 4. Relation between PING rhythm and mean firing rate in a reduced network of E and type II I cells. A: schematic overview of the recurrent network with reduced topology to simulate PING oscillations. There is no external input to the I cells. B: frequency of PING rhythm as a function of current $I_{0,E}$ and noise σ_E . Insets: raster plots (red for E cells, blue for I cells) showing the spiking activity for the same noise σ_E and low (a) and high (b) driving current $I_{0,E}$. Parameter settings: $\sigma_E = 20 \text{ mV}$ and $I_{0,E} = 0 \mu\text{A}/\text{cm}^2$ and $2.3 \mu\text{A}/\text{cm}^2$ for insets a and b, respectively. C: mean firing rate of E (left) and I (right) cells. White areas in B and C correspond to parameter values without rhythmic firing.

periodic oscillations for type I interneurons (cf. the white region in Fig. 4, B and C, bottom left) as well as for type II interneurons (Fig. 5) since the small input is not sufficient to drive the E cells above their spiking threshold. If the noise increases, more E cells are activated (see Fig. 4C and Fig. 5B), thereby eliciting PING rhythms (Fig. 4B and Fig. 5A). The lower the value of $I_{0,E}$, the higher the value of σ_E that is required to generate PING rhythms (boundary between the white and colored regions in Fig. 4B and Fig. 5A). When the constant input $I_{0,E}$ increases, the mean firing rate of the E cells increases (Fig. 4C and Fig. 5B for type I and type II interneurons, respectively). When $I_{0,E}$ increases, passing the value of $0.5 \mu\text{A}/\text{cm}^2$, we observe relatively sharp transitions of frequency (Fig. 4B and Fig. 5A), of the mean firing rate of the E

cells (MFR_E) (Fig. 4C, left, and Fig. 5B, left), and of the mean firing rate of the I cells (MFR_I) (Fig. 4C, right, and Fig. 5B, right). The transitions are caused by the transition of the E cells to the intrinsically oscillatory regime at this value of driving current. When $I_{0,E}$ increases further, so does the frequency of the PING rhythm and the firing rate of the I cells (Fig. 4, B and C, and Fig. 5, A and B, for type I and type II interneurons, respectively). For small values of noise σ_E the firing rate of the E cells is slightly less than that of the I cells (Fig. 4C and Fig. 5B). Increasing the noise to the E cells reduces the firing rate of the E cells but increases the firing rate of the I cells and the PING frequency. This can only be observed for relatively large values of $I_{0,E}$. For small values we are in the fluctuation-driven regime where the E cell firing rate slightly increases with σ_E (Brunel 2000). As the external current $I_{0,E}$ increases, the coherence among the E cells also increases. For small values of $I_{0,E}$ (E cells in the fluctuation-driven regime) the coherence weakly increases with noise; for larger values of $I_{0,E}$ (E cells in the mean-driven regime) the coherence generally decreases with noise. For low noise and larger $I_{0,E}$ the coherence is near 1. The results in Figs. 4 and 5 show that PING rhythms depend on $I_{0,E}$ and σ_E in a very similar way for both types of interneurons. The increase of firing of the E cells as a function

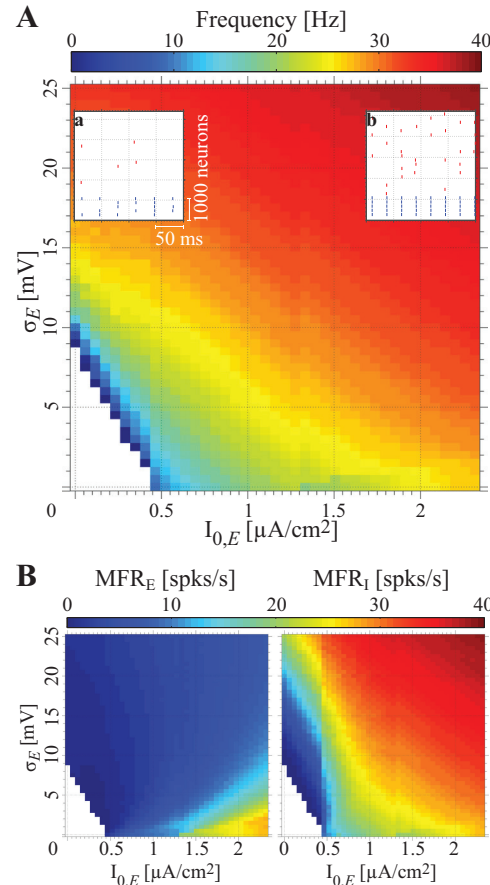


Fig. 5. PING rhythms and mean firing rate in a reduced network of E and type II I cells. The network topology is as displayed in Fig. 4A. A: frequency of PING rhythm as a function of current $I_{0,E}$ and noise σ_E . Insets a and b: raster plots (red for E cells, blue for I cells) as in Fig. 4B. B: mean firing rate of E (left) and I (right) cells. White areas in A and B correspond to parameter values without rhythmic firing. Parameter settings: $\sigma_E = 20 \text{ mV}$ and $I_{0,E} = 0 \mu\text{A}/\text{cm}^2$ and $2.3 \mu\text{A}/\text{cm}^2$ for insets a and b, respectively.

of the drive $I_{0,E}$ to the E cells will come back in Figs. 6 and 7, where we show the firing rate of the E cells, when ING and PING interact.

Interactions Between ING and PING

In the previous sections, we have considered networks with a reduced topology to study ING and PING oscillations separately. We now focus on the interaction between ING and PING rhythms. More precisely, we ask the question: If according to its connectivity the network is in principle able to generate PING as well as ING rhythms, which of the two will it generate, or will it generate a mixture? To answer this question we study the oscillation characteristics of the complete network (Fig. 6A) and compare the results with the results obtained above for ING and PING rhythms in reduced networks. In other words, we investigate whether the network oscillations change when one of the mechanisms is disabled by eliminating the projections from the pyramidal cells to the inhibitory neurons (ING) or by eliminating the input to the interneurons (PING). In particular, if network oscillations are left unchanged when disabling one mechanism and they are affected when disabling the other, we may conclude that only the other mechanism is responsible for the network oscillations in the full network.

Figure 6 shows the results for the network with type I WB neurons. The full model is schematically displayed in Fig. 6A. Figure 6B shows the frequency of network oscillations as a function of the external constant drive $I_{0,E}$ to the E cells and the external constant input $I_{0,I}$ to the I cells for 1) the ING-generating network as in Fig. 2A (blue surface), 2) the PING-generating network as in Fig. 4A (red surface), and 3) the full network as in Fig. 6A (green surface). The green surface in Fig. 6B is always equal to or slightly above the higher of the ING and PING surfaces. For small values of $I_{0,I}$ the oscillation frequency of the full network is slightly higher than the oscillation frequency of the PING mechanism. This is illustrated in detail in Fig. 6C, left, which shows the oscillation frequency for ING (blue line), PING (red line), and the full network (green line) as a function of the input $I_{0,I}$ to the I cells for a constant input $I_{0,E} = 2 \mu\text{A/cm}^2$ to the E cells, while the mean firing rate of the pyramidal cells (MFR_E, dark green line) and of the interneurons (MFR_I, light green line) corresponding to the full network (green line) are illustrated in Fig. 6C, right. The slightly higher frequency for the full model can be explained by the fact that the input from the E cells to the I cells due to the projections $g_{E \rightarrow I}$ is not suprathreshold and does not generate a spike immediately after arrival of the input spike. Larger inputs $I_{0,I}$ increase the excitability of the I cells, such that the interval between arrival of the spike volley from the E cells to the I cells and spiking of the I cells decreases. If the interval between firing of the E cells and I cells decreases, the inhibition from the I cells to the E cells comes earlier in the firing cycle of the E cells and thus has a smaller impact. The earlier start and end of the inhibition explain the reduced interval between subsequent spikes for the E cells for the full network and the corresponding higher frequency. We note that we interpreted the relation between $I_{0,I}$ and the pure PING network (Fig. 6C, left, red) as follows: There is no external input to the I cells, so the value of this parameter does not influence the PING dynamics. An alternative interpretation is

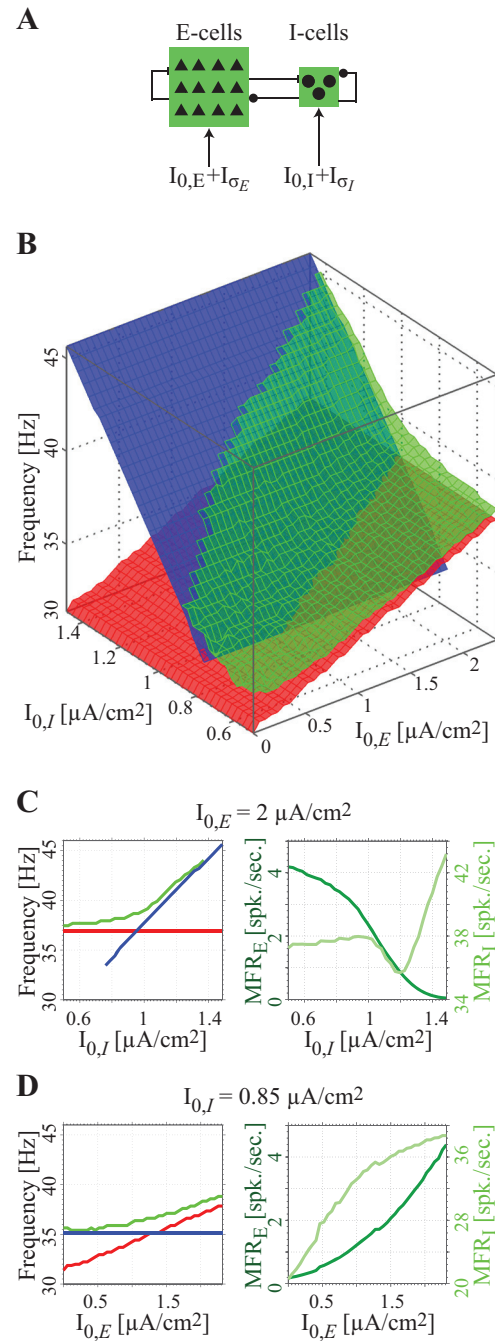


Fig. 6. Oscillations in a full network of reciprocally coupled pyramidal cells and type I interneurons. A: network topology of the full network. B: frequency of ING rhythm generated by the network in Fig. 2A (blue surface), PING rhythm generated by the network in Fig. 4A (red surface), and rhythms generated by the full network (green surface) as a function of mean current to E cells ($I_{0,E}$) and to I cells ($I_{0,I}$). When the green and blue surfaces closely overlap (for large values of $I_{0,I}$ and small values of $I_{0,E}$), only the blue surface is shown. C and D, left: cross sections of B along the $I_{0,I}$ (C) and $I_{0,E}$ (D) axes for fixed $I_{0,E}$ (C) and fixed $I_{0,I}$ (D). Right: corresponding mean firing rates of the interneurons (light green) and of the pyramidal cells (dark green). Parameter values: $\sigma_E = 20 \text{ mV}$ and $\sigma_I = 0.5 \text{ mV}$.

to assume $I_{0,I} = 0 \mu\text{A/cm}^2$ for pure PING. Then, the continuation of the red surface in Fig. 6B and the red line in Fig. 6C, left, to nonzero values of $I_{0,I}$ should be viewed as reference for comparison.

When $I_{0,1}$ increases in Fig. 6C, *left*, the oscillation frequency of the full network approaches that of the pure ING oscillations while the corresponding MFR_E monotonically decreases (Fig. 6C, *right*). The transition from PING-dominated responses to ING-dominated responses is gradual for the network with the type I interneurons, in agreement with earlier results by Börgers and Walker (2013). Although the full network generates ING-dominated oscillations for higher values of $I_{0,1}$, the pyramidal cells are still active (see Fig. 6C, *right*). The higher oscillation frequency for the full network at the transition of the blue and red lines in Fig. 6C, *left*, is explained by the fact that the interneurons receive input from the pyramidal cells in the full model, and thereby receive more excitation for the same value of $I_{0,1}$ than for the ING condition. This larger amount of excitation causes a higher oscillation frequency in the network of interneurons and thereby also a higher oscillation frequency for the full network.

Note that although MFR_E is low for high values of $I_{0,1}$ (Fig. 6C, *right*), we observe clear gamma rhythms in the pyramidal cells. The MFR_I in Fig. 6C, *right*, varies in a more complicated way with changes in $I_{0,1}$ than the rate of the pyramidal cells (MFR_E). First MFR_I slightly increases, then decreases, and increases again as $I_{0,1}$ increases. This can be understood as follows: For small values of $I_{0,1}$ many E cells recover from the inhibition sooner than the I cells do and start spiking to elicit spiking of the I cells. We observe a PING rhythm. The I cells spike once in each oscillatory cycle, and their mean firing rate increases like the frequency of the full network as $I_{0,1}$ increases. As $I_{0,1}$ increases further, the increased excitation to the I cells lets some I cells recover sooner from the inhibition than the E cells. These inhibit the E cells, in particular the E cells in the population that tend to fire late. This leads to less excitation given to the I cells from the E cells and therefore to a lower mean firing rate of the I cells. We checked that the higher the noise σ_I , the more I cells recover early and the stronger the effect. When $I_{0,1}$ increases even further, the I cells receive more excitation and further inhibit the E cells until the excitation from the E cells is so low that the full network behaves like pure ING, i.e., the mean firing rate of the I cells increases and the I cells skip a lower number of the oscillatory cycles as $I_{0,1}$ increases.

Figure 6D, *left*, shows the oscillation frequency for ING (blue line), PING (red line), and the full network (green line) as a function of the input $I_{0,E}$ to the E cells for a constant input $I_{0,1} = 0.85 \mu\text{A}/\text{cm}^2$ to the I cells, while Fig. 6D, *right*, shows the mean firing rate of the pyramidal cells (MFR_E , dark green line) and of the interneurons (MFR_I , light green line) corresponding to the full network (green line in Fig. 6D, *left*). For small values of $I_{0,E}$ the oscillation frequency for the full network is close to the ING oscillation frequency while the pyramidal cells show clear gamma rhythms although MFR_E is low (see Fig. 6D, *right*). For larger values of $I_{0,E}$ near the intersection of the red and blue lines the oscillation frequency of the full network (green line) (Fig. 6D, *left*) exceeds that for ING and PING rhythms for the same reasons as for Fig. 6C, *left*. For larger values of $I_{0,E}$ the oscillation frequency of the full model increases with the pure PING oscillation frequency (and so does the mean firing rate of the pyramidal cells and of the interneurons) but always remains somewhat higher than the pure PING frequency. The latter is in agreement with results by Börgers and Walker (2013), who reported that increase of input

to the E cells in a network of reciprocally coupled E and I cells advances firing of the I cells in each cycle when their phase response is of type I.

Summarizing, our results show that the oscillation frequency of the full network is equal to (or somewhat higher than) the higher of the pure ING and pure PING oscillation frequencies. The reason for this is that the higher-frequency mechanism recruits the vast majority of available neurons in the two populations, such that the other mechanism cannot exist. For example, when the PING frequency is higher than the ING frequency, the E neurons recover before the I neurons; they spike and recruit the I neurons into the PING rhythm by near-suprathreshold excitation. The ING rhythm then cannot develop, because the I neurons cannot reach threshold because of their intrinsic drive. In contrast, when the ING frequency is higher than the PING frequency, the I neurons recover before the E neurons and are reset when the input from nonsuppressed E neurons arrives, such that they cannot be recruited into the PING rhythm.

Figure 7 shows an analysis similar to Fig. 6 for the network with type II interneurons. As in the analogously structured Fig. 6, the blue, red, and green surfaces in Fig. 7A represent the firing frequencies for pure ING oscillations ($g_{E \rightarrow I} = 0 \text{ mS}/\text{cm}^2$), for pure PING oscillations ($I_{0,1} = 0 \mu\text{A}/\text{cm}^2$), and for the full network, respectively, while the dark green and light green curves in Fig. 7B, *right*, represent the mean firing rate of the pyramidal cells and of the interneurons in the full network. The main difference between the results in Fig. 7A for type II interneurons and the results in Fig. 6B for type I interneurons is that the firing frequency of the full network can be between that of ING and PING for type II interneurons for intermediate values of $I_{0,E}$ and $I_{0,1}$ (compare also Fig. 6C, *left*, and Fig. 7B, *left*). The explanation for this observation is that when the ING rhythm dominates the E cells can only fire just before firing of the I cells, i.e., before inhibition from the interneurons comes in. The action potentials from the E cells then arrive at the I cells just after their firing, which causes a phase delay because of the type II PRC, and therefore a lower frequency of the full network compared with the pure ING frequency. When the input $I_{0,1}$ increases to larger values, the frequency of the full network becomes fully determined by the ING frequency (Fig. 7, A and B, *left*) while the mean firing rate of the pyramidal cells of the full network strongly decreases. In that case the blue and green surfaces (Fig. 7A) or curves (Fig. 7B, *left*) overlap. This holds even though the E cells are still active near the transition, albeit with reduced frequency (Fig. 6C and Fig. 7B, *right*). The blue line for ING in Fig. 7B, *left*, shows some abrupt variation, which may suggest an underlying bifurcation.

When the I drive is even stronger, the E cells become suppressed (cf. Börgers and Kopell 2003, 2005; Börgers and Walker 2013). In this sense, our transition for increasing I drive may be considered as a part of the suppression transition. Like Börgers and Walker (2013), in networks with type II interneurons we find a rather abrupt departure from PING oscillations when increasing the I drive (green curve in Fig. 7B, *left*). For different transition paths (increasing the E drive; see Fig. 7C) the transition is more gradual. Figure 7C, *left*, shows the oscillation frequency when the input to the interneurons is constant and when the input $I_{0,E}$ to the E cells is varied; for small values of $I_{0,E}$, the oscillation frequency of the full network (green curve) is slightly below that for the ING

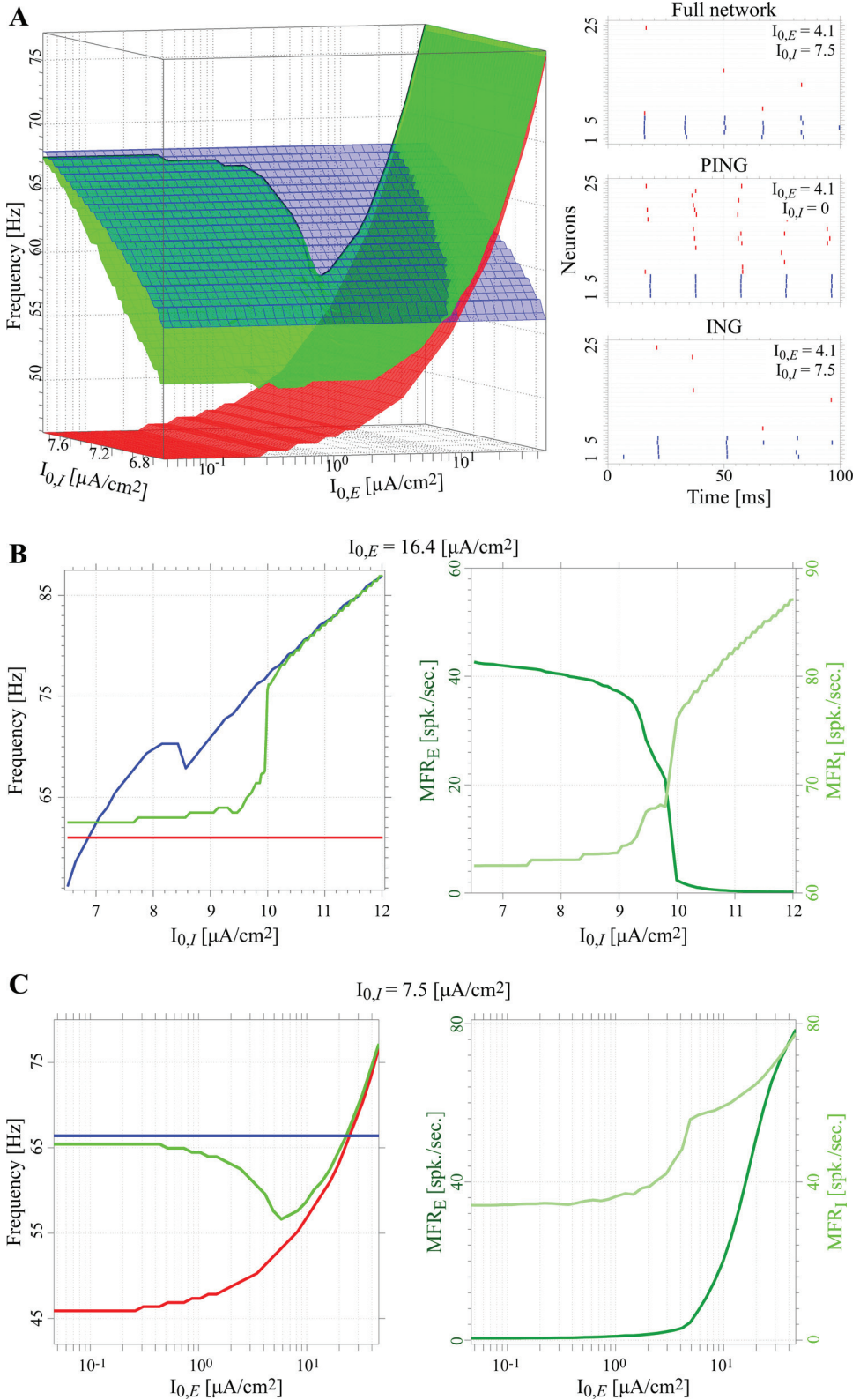


Fig. 7. Oscillations in a full network of reciprocally coupled pyramidal cells and type II interneurons. Network topology is as in Fig. 6A. *A*: frequency of ING rhythm generated by the network in Fig. 2A (blue surface), PING rhythm generated by the network in Fig. 4A (red surface), and rhythms generated by the full network (green surface) as a function of mean current $I_{0,E}$ to E cells and $I_{0,I}$ to I cells. Raster plots show the firing of the E (red) and I (blue) neurons for the full network and the reduced PING and reduced ING networks, at the same point in parameter space. *B* and *C*, *left*: frequency for ING (blue line), PING (red line) and the full network (green line). *Right*: mean firing rate of the interneurons (light green) and of the pyramidal cells (dark green) for variations in $I_{0,I}$ (*B*) and $I_{0,E}$ (*C*). Parameter values: $\sigma_E = 60$ mV and $\sigma_I = 0.5$ mV.

rhythm (blue curve), again because of the effective delaying of I cells through E cells as explained above. When $I_{0,E}$ increases, the oscillation frequency of the network (green line) decreases, approaching the pure PING oscillation frequency (red line) even when the pure PING oscillation frequency is lower than the pure ING oscillation frequency.

From there the frequency of network oscillations follows the frequency of PING oscillations.

The reason for the fact that in intermediate input ranges in Fig. 7, *A* and *C*, *left*, the full network approaches the pure PING oscillation frequency as $I_{0,E}$ increases even when the pure ING oscillation frequency is higher lies again in

the phase delay in the PRC of type II interneurons: During the full network ING rhythm, the E cells spike such that their input arrives early in the phase of the I neurons, so it has a delaying effect and reduces the frequency of the ING rhythm. In other words, when the oscillation frequency for the full network is between pure ING and pure PING, the type II nature of the interneurons causes a lower frequency for ING in the full network than in the reduced network, such that the higher frequency is in fact PING; this dominates the network oscillations in the full network. So, as in networks with type I interneurons, we have in fact the higher frequency generating mechanism winning.

When the external input to the E cells increases, the mean firing rate of the E cells increases (see Fig. 7C, right). The higher mean firing rate of the E cells implies that the E cells provide more excitation to the I cells. This larger amount of excitation arrives at early phases in the firing cycle of the I cells and gives rise to a larger phase delay (lower firing rate) of the I cells due to their type II PRC. Because of the larger phase delay of the I cells, the interval of firing of the I cells decreases. This explains why the frequency of the full network (green line in Fig. 7C, left) decreases as $I_{0,E}$ increases.

Given the decrease in the frequency of the full network, it may seem contradictory that the mean firing rate of the I cell increases as $I_{0,E}$ increases (Fig. 7C, right). The explanation is that the increased firing of E cells provides more excitation to the I cells, such that more I cells fire in each cycle, which becomes longer. The frequency of the full network decreases until it approximately meets the pure PING frequency (see Fig. 7C, left): At this point, $I_{0,E}$ increases the excitability of the E cells high enough such that the E cells recover from the inhibition from the I cells sooner than the

I cells and the full network generates PING-dominated oscillations.

Analytical Insights into Interactions Between ING- and PING-Driven Oscillations with a Phase Model

The results of the computer simulations presented so far might raise the question of whether these results are generic and not due to a particular choice of parameter values in our model. To address this issue, we performed a mathematical analysis of a simple pair of neurons with an excitatory (E) and an inhibitory (I) neuron (see METHODS). This simple model allows for analytical expressions for the firing rate of the system for various conditions (see APPENDIX). Since we want to investigate the interaction between ING and PING on network oscillations we provide input to both the E and I neurons in our simulations. From the previous sections and from the literature (e.g., Börgers and Kopell 2003, 2005; Börgers and Walker 2013) we know that PING will dominate the network dynamics for relatively large input to the E neuron and small input to the I neuron and that ING dominates when the input to the E neuron is relatively small and the input to the I neurons is large. We are interested in intermediate regimes of transition between PING and ING, far from these extremes. More precisely, we focus on regimes where both the E and the I neuron spike once in every cycle. In particular, also during ING-dominated oscillations the E neuron should not be suppressed but it should generate a regular spike rhythm with one-to-one locking. This restricts the ranges of admissible parameters.

For an illustration of this case, see Fig. 8A, which shows the firing of the E neuron (red vertical lines) and I neuron (blue vertical lines) for the ING condition. The figure shows results for model 1 (see METHODS), where the E and I neurons are both LIF neurons. If the E neuron (red trace in Fig. 8A) fires in this

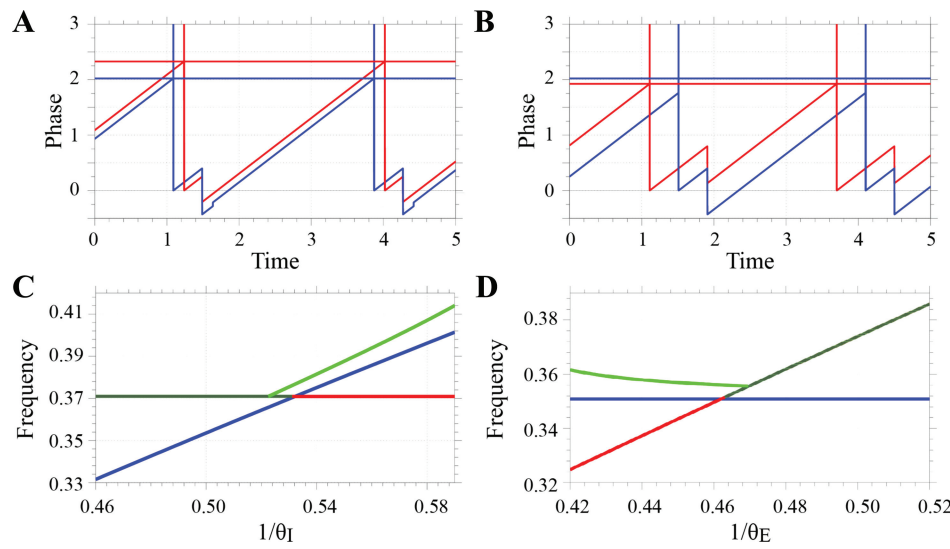


Fig. 8. Interactions between ING and PING oscillations for an LIF-LIF phase model. **A** and **B**: examples of ING-dominated phase dynamics (**A**) and PING-dominated phase dynamics (**B**) as a function of time (arbitrary units) for a network with 2 LIF neurons coupled by excitation and inhibition. The firing of the E (I) neuron is indicated by red (blue) vertical lines. The time delay from the E neuron to the I neuron is equal to that from the I neuron to the E neuron (0.4 units; if the firing rate were 40 Hz, the delay of 0.4 units would correspond to ~ 3 ms). **C**: firing frequency of the network as a function of the input to the I neuron while the input to the E neuron is kept constant. Blue and red lines show the network oscillations for pure ING and pure PING, respectively. Green curve shows the frequency of network oscillations for the full 2-neuron network; dark green indicates full-network PING and light green full-network ING. **D** similarly shows the network oscillations as a function of the input to the E neuron, while the input to the I-neuron is kept constant. For the full network the parameter values for the coupling strengths are $\varepsilon_{I \rightarrow E} = -0.5$, $\varepsilon_{E \rightarrow I} = 0.1$, $\varepsilon_{I \rightarrow I} = -1.0$, and $\tau = 0.4$; for the ING condition we set $\varepsilon_{E \rightarrow I} = 0$, which eliminates any input from the E to the I neuron. The input to the I and E neurons is $1/\theta_I = 0.495$ and $1/\theta_E = 0.43$ for **A**, $1/\theta_I = 0.495$ and $1/\theta_E = 0.52$ for **B**, $1/\theta_E = 0.495$ for **C**, and $1/\theta_I = 0.495$ for **D**.

ING condition, either it fires just before the I neuron (blue trace) with a time lead smaller than the conduction delay τ from the E neuron to the I neuron or the E neuron fires just after firing of the I neuron before the inhibition of the I neuron arrives at the E neuron. Figure 8A illustrates the latter case. The self-inhibition of the I neuron is reflected by the inhibition in the blue trace in Fig. 8A at a time τ ($= 0.4$ time units) after firing of the I neuron; similarly, the excitation from the E neuron to the I neuron is reflected by the small increment in the blue trace at time 0.4 after firing of the E neuron.

Figure 8B shows the relative firing of the E and I neurons for the PING condition. After firing of the E neuron, the I neuron fires with a delay τ , i.e., the output from the E neuron raises the phase of the I neuron above the phase threshold Θ_I near the value 2. The I neuron will then send inhibitory output back to the E neuron and to itself. This is illustrated by the decrease of the phase of the E and I neurons at time 2τ after firing of the E neuron.

The frequencies of the ING and PING oscillations can be computed analytically. Figure 8C displays the results (Eqs. A2, A4, and A5 with Eqs. A6 as well as A7) as a function of the free firing frequency of the I neuron. This firing frequency is a unique, monotonically increasing function of the constant input to the interneuron. The blue line in Fig. 8C shows the network oscillation frequency for the pure ING condition ($\varepsilon_{E \rightarrow I} = 0$, cf. APPENDIX). This increases linearly when the input to the interneuron measured by $1/\theta_I$ increases, in agreement with previous studies (Bartos et al. 2001, 2007). The red line in Fig. 8C shows the network oscillation frequency for pure/ideal PING with suprathreshold excitation of the I neuron (cf. APPENDIX). For the full model, the frequency of rhythmic activity for different constant inputs to the I cell is illustrated by the green curve in Fig. 8C. For small inputs to the I cell, PING dominates the behavior of the model (dark green part of the green curve), which explains why the green and red lines superimpose at the left-hand side of Fig. 8C. When the input to the I cell increases such that the firing frequency of the I cell exceeds that of the E cell ($1/\theta_I \approx 0.53$), ING takes over (i.e., the full network generates an ING rhythm, light green part of the curve) and the frequency of the rhythm of the full model increases, similar to that of pure ING. This happens because the I cell recovers from the inhibition before the E cell does, it delays spiking of the E cell, and determines the rhythm. The firing rate of the network exceeds that of pure ING because the I cell in the full network also receives additional excitatory input from the E cell. Figure 8 illustrates that the network oscillation frequencies approximately follow the firing frequencies of pure ING or PING, whichever is the largest of the two. This agrees with our results from the computer simulations for the model with the single-compartment Hodgkin-Huxley type I neuron model in Fig. 6C, *left*. The reason for this is that the higher-frequency mechanism recruits both available neurons just as it recruits the majority of neurons in the large two-population networks, such that the other mechanism cannot exist.

Interestingly, the theoretical analysis reveals a small region of bistability for values of $1/\theta_I$ between ~ 0.52 and 0.53 (see Fig. 8C): When the constant input to the I neuron gradually increases, the model generates the pure PING-firing frequency until the blue ING line intersects the red PING line (cf. the dark green line). At that crossing, the model switches to ING and to the firing rates along the light green curve. When the input to

the interneurons is gradually decreased starting from high values, the firing frequency follows the light green curve until it intersects the red line. From there the firing frequency of the model follows the red pure PING line (dark green line). We do not observe such a region in the larger networks, maybe because effects of coupling inhomogeneity and noise do not allow a sufficient separation of the close-by frequencies.

Figure 8D shows the changes in frequency of the rhythmic activity when the input to the E cell is varied while the input to the I neuron is kept the same. The frequency of the rhythmic activity is obtained from Eqs. A2, A4, and A5 with Eqs. A6 as well as A7. The red line in Fig. 8D illustrates the increase of pure PING frequency with increasing input to the E cell (note that the green curve superimposes the red line for larger inputs). This is a direct consequence of the increase in firing rate of the E cell when it receives increasing input. Pure ING oscillations are not affected by changes in input to the E cell (blue line in Fig. 8D). For small input to the E neuron (with $1/\theta_E$ approximately less than 0.46) the full network generates ING-dominated oscillations with a frequency that is approximately constant despite variations in input to the E cells (light green line); this happens when the firing frequency for the pure PING case (red line) is below that for the pure ING case (blue line) (Fig. 8D). As in Fig. 8C, the higher frequency “wins.” The frequency of the full model ING exceeds the frequency of the reduced-network ING rhythm, because the full model has projections from the E to the I cell, which provide excitatory input in addition to the constant input to the I cell. When the network frequency for reduced-network PING exceeds that of reduced-network ING, the full network adopts the PING rhythm (dark green line superimposed on red line in Fig. 8D). In between there is again a small region of coexistence. These results are in good agreement with the results of the simulations of larger networks with single-compartment Hodgkin-Huxley type I neurons (cf. Fig. 6D, *left*).

Figure 9 shows the results for the network where the I neurons are represented by a type II sine neuron. As in Fig. 8, Fig. 9A shows the firing of the E (red) and I (blue) cells for ING-dominated firing of the network. The firing of the E cell precedes the firing of the I cell, but the interval between their spikes is less than the time delay τ from the E to the I neuron (0.4). Therefore, firing of the I cell is due to its intrinsic firing and not an immediate consequence of excitation by the E cell. In fact, the excitation of the I cell by spike input from the E cell is hardly visible because of the nature of the sine neuron: An excitatory input arriving just after the I cell’s reset causes a rather small delay in firing, not a marked depolarization. The inhibition of the E cell after firing of the I cell is clearly visible, simultaneous with the increase of the phase of the I cell by self-inhibition, which, because of the type-II PRC of the sine neuron, leads to a phase advance (i.e., an increase of the membrane potential). Figure 9B shows the same results for a PING rhythm in the circuit.

Figure 9, C and D, show the frequency of ING (blue line), PING (red line), and the full model (green line) according to Eqs. A3, A4, A9, and A11. In Fig. 9C we vary the input $1/\theta_I$ to the I neuron with fixed input $1/\theta_E$ to the E neuron. In Fig. 9D the input $1/\theta_E$ to the E neuron is varied while the input $1/\theta_I$ to the I neuron is kept constant. In both Fig. 9, C and D, the frequency of the full network is between the frequencies of the pure ING and pure PING rhythms. Nevertheless, the full

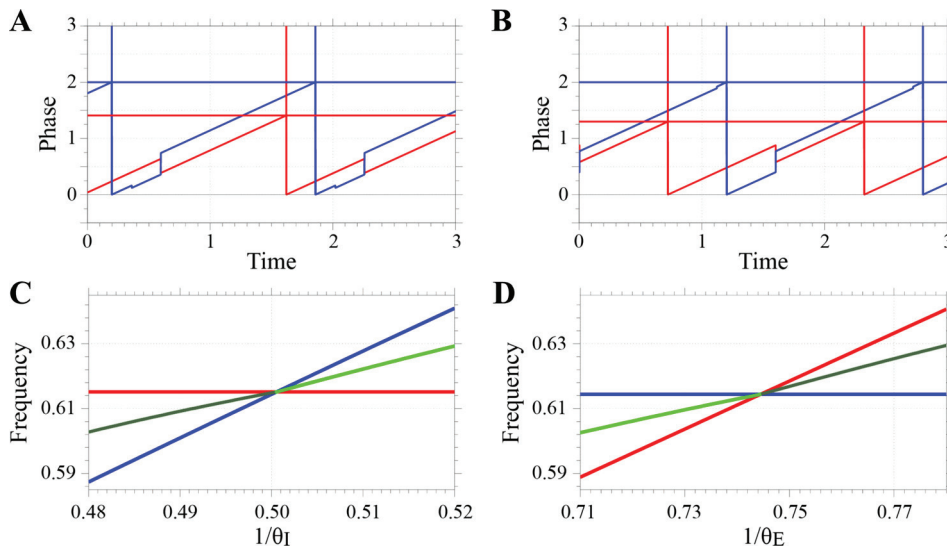


Fig. 9. Interactions between ING and PING oscillations for the LIF-sine phase model. *A* and *B*: examples of ING-dominated phase dynamics (*A*) and PING-dominated phase dynamics (*B*) as a function of time (arbitrary units) for a network with a LIF-type E neuron and a sine neuron as I cell. The firing of the E (I) neuron is indicated by red (blue) vertical lines. The time delay from the E neuron to the I neuron is equal to that from the I neuron to the E neuron (0.4 units as in Fig. 8). *C*: firing frequency of the network when the input to the E cells remains constant. Blue and red lines show the network oscillation frequencies for pure ING and pure PING, respectively. Green curve shows the frequency of network oscillations for the full 2-neuron network; dark green indicates full-network PING and light green full-network ING. *D* is similar to *C*, except that the input to the I neuron is constant while the input to the E neuron varies. For the full network, the parameter values for the strengths of the couplings are $\varepsilon_{I \rightarrow E} = -0.2$, $\varepsilon_{E \rightarrow I} = 0.1$, $\varepsilon_{I \rightarrow I} = -0.42$, and $\tau = 0.4$; input from the E to the I neuron was eliminated to obtain ING by setting $\varepsilon_{E \rightarrow I} = 0$. The input to the I and E neurons was $1/\theta_I = 0.5$ and $1/\theta_E = 0.71$ for *A*, $1/\theta_I = 0.5$ and $1/\theta_E = 0.77$ for *B*, $1/\theta_E = 0.75$ for *C*, and $1/\theta_I = 0.5$ for *D*.

network generates either ING or PING depending on which mechanism (pure ING or pure PING) yields the higher-frequency oscillations in the reduced networks (cf. dark and light green parts of the green curve highlighting PING and ING oscillations in Fig. 9, *C* and *D*, respectively). Already for inputs to the I neuron that are smaller than those to the E neuron, the frequency of the PING rhythm exceeds that of the ING rhythm, i.e., the red line lies above the blue line [see the results for $1/\theta_I < 0.5$ ($1/\theta_E = 0.75$) in Fig. 9*C* and $1/\theta_E > 0.74$ ($1/\theta_I = 0.50$) in Fig. 9*D*]. We can see from the detailed dynamics of the full network in Fig. 9*B* that in this case the E cell recovers from reset and inhibition before the I cell does and it excites the I cell to spiking, i.e., the full network generates PING oscillations. The oscillation frequency is nevertheless between those of pure PING and pure ING. This can be understood from the fact that we assumed an “ideal” PING rhythm for the comparison, in the sense that the input from the E cell to the I cell is practically suprathreshold, causing the I neuron to fire immediately after arrival of the E spike. Our type II neuron does not allow for strictly suprathreshold input, i.e., our type II neuron requires an infinitely strong input pulse to immediately reach threshold. For the full model, the I cell will spike shortly, but not immediately after arrival of the E spike. The small delay in firing causes a delay in arrival of inhibition at the E cell, a larger impact of the inhibitory input and therefore a delay in the next spike of the E cell. The frequency of the rhythm of the full network is then below that of the pure PING rhythm. The observation that the frequency of the full network is higher than the frequency of pure PING may be understood from the fact that the frequency of pure PING is higher than the frequency of pure ING: This implies that during the full-network PING rhythm the E neuron reaches the threshold for firing faster than the I neuron. When the threshold for firing of the E neuron is reached, the spike from the E neuron arrives at

the I neuron in the second half of its phase cycle. This causes a phase advance for the I neuron, causing a higher firing rate for the I neuron than for the pure ING case.

For relatively large inputs to the E neuron (or small inputs to the I neuron), the phase model with type II interneuron yields results (Fig. 9, *C* and *D*) that are qualitatively different from the results for the network with Hodgkin-Huxley type II neurons shown in Fig. 7: For the phase model the frequency of the full network is lower than the frequency of PING (see Fig. 9, *C* and *D*), whereas it is slightly higher for the Hodgkin-Huxley type model (see Fig. 7, *B* and *C*, left). This discrepancy stems from the fact that for the phase model with type II interneuron the synaptic strength $\varepsilon_{E \rightarrow I}$ from the E to the I neuron for pure PING is assumed to be larger than that for the full network to generate the “ideal” PING rhythm with practically suprathreshold input. However, the synaptic connectivity $\varepsilon_{E \rightarrow I}$ is the same for pure PING and for the full network for the Hodgkin-Huxley-type model. When $\varepsilon_{E \rightarrow I}$ is larger for pure PING than for the full network in the phase model, the interneuron will spike at shorter latencies after a spike by the E neuron for PING than for the full network. As a consequence, the firing rate will be higher for PING than for the full network. However, in the case of the Hodgkin-Huxley-type model where the effective strength of outputs from the pyramidal cells to interneurons in PING and in the full network is approximately the same, the interval between spiking of the E and I neurons is approximately the same. Frequency differences between pure PING and full-network PING are a consequence of the additional external inputs to interneurons. Because interneurons in the full network receive additional constant inputs $I_{0,I}$ that are not present or negligible in case of pure (reduced network) PING, the frequency of the Hodgkin-Huxley full network is higher.

For small input to the E neuron (or large input to the I neuron), the frequency of pure ING oscillations exceeds that of pure PING oscillations (see Fig. 9, *D* and *C*, left and right, respectively). In these cases, the full network generates ING oscillations. Again, this is because the I cell recovers faster from the reset and excitation-inhibition than the E cell does. The frequency of the full network is nevertheless lower than that of pure ING. This can be understood as follows. During the full-network ING rhythm, the excitatory output from the E neuron arrives at the I neuron in an early phase of the I neuron, which causes a phase delay for the type II interneuron, see, e.g., Fig. 9A. The period of the full network is then longer than the period of pure ING, or in other words, the frequency of the full network is lower than the frequency of pure ING. Furthermore, when the I neuron spikes, inhibition from the I neuron arrives at the E neuron at a phase $< 2\tau$ for the full network but at the phase 2τ of its cycle for pure PING. Because of the shape of the PRC of the E neuron, inhibition generated by the I neuron then delays the spiking of the E neuron in the full network less than in case of the reduced network generating pure PING and the E neuron in the full network recovers from the inhibition sooner than the E neuron in the pure-PING reduced network does. The period of the full network is then shorter than the period of PING, i.e., the frequency of the full network exceeds that for PING. This agrees with the studies based on the Hodgkin-Huxley-type model (see Fig. 7).

DISCUSSION

We have investigated the interactions between gamma oscillations generated by ING and PING mechanisms, using a model inspired by neural networks in hippocampal region CA1. Usually ING oscillations have been studied in networks with input to interneurons without drive to pyramidal cells (if present at all in the network). Similarly, PING oscillations have usually been studied in networks of mutually coupled pyramidal cells and interneurons with external input to the pyramidal cells but without external input to the interneurons. In this study we have investigated network oscillations when both ING and PING can in principle be generated because of the network connectivity and the external input to both the pyramidal cells and the interneurons. We have investigated PING and ING oscillations and oscillations in the full network where ING and PING interact. In our study we considered both networks with type I and networks with type II interneurons. Our results are derived with computer simulations of networks with pyramidal cells and interneurons as well as analytical considerations for simple two-neuron circuits. Analyzing the similarities and differences between the dynamics of the two setups allows a better understanding of the dynamics. Furthermore, the approach demonstrates that the simulation results reflect a general behavior of networks with pyramidal cells and interneurons rather than a particular behavior that is specific for a small niche in parameter space used in the computer simulations.

The results in Figs. 2 and 3 show that gap-junctional coupling may be sufficient to generate ING oscillations in our networks of coupled interneurons, for both type I and type II interneurons, well in agreement with previous observations (Chow et al. 1998; Chow and Kopell 2000; Galarreta and Hestrin 1999, 2001a, 2001b; Gibson et al. 1999, 2005; Kopell

and Ermentrout 2004). We find a richer dependence of the oscillations on the inhibitory coupling than previously reported: For type I interneurons the frequency of ING oscillations decreases when the inhibition increases, while the coherence increases (Fig. 2, *B* and *C, right*). At some value, the ING oscillation frequency abruptly increases before the oscillation disappears and reappears for larger values of synaptic strength $g_{I \rightarrow I}$ (see Fig. 2B). Studies on two-neuron systems (see Bem and Rinzel 2004; Canavier et al. 2013; Di Garbo et al. 2002, 2007a, 2007b; Ermentrout 1996; Ernst et al. 1995; Jeong and Gutkin 2005; Lewis and Rinzel 2003; Merriam et al. 2005; Meyrand et al. 2009; Nomura et al. 2003; Nomura and Aoyagi 2005; Oh and Matveev 2009; Pfeuty et al. 2005; Terman et al. 1998, 2011; van Vreeswijk et al. 1994) have not reported such findings, likely because they did not consider self-inhibition. Nevertheless, there are some similarities between our results and their results for intermediate values of $g_{I \rightarrow I}$. Lewis and Rinzel (2003) reported bistability for interneurons coupled by gap junctions and chemical synapses without self-inhibition. We also find in two-neuron simulations with self-inhibition and parameters adapted to describe the two neuron populations in our large networks that in-phase and antiphase firing coexist for intermediate values of $g_{I \rightarrow I}$, related to the region without oscillations (white area) in the full network with $g_{I \rightarrow I} = 4 \times 10^{-3}$ - 10^{-1} mS/cm² in Fig. 2B. Furthermore, we verified that a system of two inhibitory coupled WB neurons with self-inhibition reveals behaviors similar to those in larger networks not only for intermediate values of $g_{I \rightarrow I}$ (range $g_{I \rightarrow I} = 4 \times 10^{-3}$ - 10^{-1} mS/cm² in Fig. 2B) but also for small ($g_{I \rightarrow I} < 4 \times 10^{-3}$ mS/cm² in Fig. 2B) and large ($g_{I \rightarrow I} > 10^{-1}$ mS/cm² in Fig. 2B) values of $g_{I \rightarrow I}$, where in-phase firing between the two neurons is preferred compared with antiphase firing. In agreement with the two-neuron systems with self-inhibition, the large networks generate synchronized firing activities for small and large values of $g_{I \rightarrow I}$, only when $g_{I \rightarrow I}$ is too small, e.g., on the order of 10^{-4} mS/cm², the large networks cannot generate synchronized firing because of noise. A pair of two inhibitorily coupled Hodgkin-Huxley-type neurons with self-inhibition was also studied by White et al. (1998a). For the parameters used in their study, White et al. (1998a) always observe in-phase synchronization between the two neurons regardless of the choices of the external drive, the strength of the inhibitory chemical synapse, and the decay time constant of the synapse. We speculate that the discrepancy (no antiphase observed) might be due to the relatively long decay time constant of the synapse used in White et al. (1998a). In this context it is interesting to point out a resemblance to the results in the work by Achuthan and Canavier (2009). The authors report that full synchrony in networks of WB interneurons can fall apart into clusters of neurons that fire in antiphase, followed by asynchrony when the strength of synaptic coupling increases to large values. In addition, our simulations show that the range of values for $g_{I \rightarrow I}$ where stable oscillations are absent becomes smaller for increasing values of gap-junctional coupling. This illustrates that synchronization by gap-junctional coupling can support oscillations by synaptic coupling, in agreement with previous results by Kopell and Ermentrout (2004) and Lewis and Rinzel (2003).

In RESULTS we used the argument that in order to create ING interneurons require a certain minimal amount of inhibition from other interneurons (Wang and Buzsáki 1996) and that the

role of inhibition might be to erase the “history” of the interneurons (see also Kopell and Ermentrout 2004). Since a population of uncoupled neurons can be synchronized by a single inhibitory pulse this has been the general view in the research community for a while, and this mechanism is thought to underlie ING-like oscillations in the gamma frequency range (30–80 Hz) in hippocampus and neocortex. In this context, it is worth noting that Börgers et al. (2010) showed that synchronization by an inhibitory pulse may fail for populations of classical Hodgkin-Huxley neurons, more likely when the hyperpolarizing inhibitory pulse is strong or long-lasting. Recently, Tikidji-Hamburyan et al. (2015) demonstrated that synchronization in resonator neurons can be robust even when the hyperpolarizing inhibition is strong, as long as the time constant of the inhibitory synapse is short enough. Both results are consistent with our study, which finds for type II neurons and hyperpolarizing inhibition variations in synchronization and coherence as a function of the strength of the inhibitory coupling, cf. Fig. 3.

For networks with type II interneurons, the dependence of ING oscillations on $g_{I \rightarrow I}$ and g_{GJ} is quantitatively and qualitatively different from that in a network with type I interneurons. The first quantitative difference is that ING oscillations occur at smaller values of gap-junctional coupling in networks with type II interneurons than in networks with type I interneurons when chemical synapses are weak or absent (see Fig. 2B and Fig. 3A). Exploratory simulations indicate that these and following observations of loss of synchrony are related to coexisting stable in-phase and antiphase oscillatory states in corresponding two-neuron systems. Another difference is that chemical synapses compete with the gap junctions to generate stable ING oscillations for type II neurons (Fig. 3) when the chemical synaptic coupling strength is small. More specifically, when the synaptic coupling increases, the value required for gap-junctional coupling to obtain ING oscillations increases.

The dynamics of PING oscillations has been addressed in many studies. Variations in external drive can create or abolish PING rhythms (see Börgers et al. 2005; Börgers and Kopell 2003, 2005; Börgers and Walker 2013). The set of parameter values taken from experimental data on CA1 networks yields stable PING oscillations in our model for both type I and type II interneurons. Moreover, the raster plots in Fig. 4B and Fig. 5A show that for sufficiently noisy conditions the population of pyramidal cells reveals a clear gamma rhythm, whereas each pyramidal cell fires once every few cycles, in agreement with experimental observations. The explanation for the finding that the firing rate of pyramidal cells in biological neural networks is considerably lower than the oscillation frequency of PING has not yet been set unambiguously. Various explanations have been suggested: Kopell and LeMasson (1994) showed that in a network with coupled excitatory and inhibitory neurons hyperpolarization-activated inward currents can help to produce population rhythms in which individual cells participate sparsely and randomly. A shift in the activation curve of such a current changes the fraction of the cells participating in any given cycle of the population rhythm. Conceptually related approaches assume cholinergic modulation, by variations in adaptation currents to produce intermittent spiking of pyramidal cells in PING rhythms (Kilpatrick and Ermentrout 2011; Krupa et al. 2014). This mechanism is related to the long-

lasting afterhyperpolarization observed in pyramidal cells (Mann et al. 2005). Another suggestion was that noise can cause low and intermittent spike discharges in pyramidal cells that interact with interneurons in PING-like rhythms (see Börgers et al. 2005; Börgers and Kopell 2005). In the present study we have used a model belonging to the second class of explanations, using Gaussian white input current noise, to yield firing rates of E cells well below the frequency of the PING rhythm. This noise input can be considered as the arguably simplest approximation to the effects of random external spike trains and as an implementation of other noise sources such as channel noise (Goldwyn and Shea-Brown 2011).

Since the main focus of our study was on the interaction between ING and PING rhythms, we showed the characteristics of ING and PING oscillations separately only for some network parameters, such as gap-junctional coupling, synaptic coupling strength, connection heterogeneity, and time-dependent input noise. A full analysis of ING and PING responses for other network parameters, such as variability in the constant drive to I and E cells, would be outside the scope of this study. However, it is relevant to mention that ING rhythms are sensitive to variations in the constant drive to the I cells and in the number of synaptic inputs. Our exploratory simulations show that the straightforward ING rhythm disappears when the variability in constant drive becomes too large. This happens more easily in the full than in the reduced network and provides another path of transition between ING and PING.

In our study we assumed connection probabilities between I cells and between E and I cells as reported in anatomical and neurophysiological studies (see METHODS). This requires some attention, since it is important to realize that connection probabilities per se are not useful. What matters more is the number of synaptic inputs per cell (see, for instance, Börgers and Kopell 2003; Golomb and Hansel 2000; Tiesinga et al. 2002). In most computer simulations, the number of neurons in the network is much smaller than in the neurophysiological substrate. Previous studies (see, e.g., Börgers and Kopell 2003; Golomb and Hansel 2000) have shown that a minimum number of synaptic inputs per cell is required to obtain synchronization. In particular, synchronous firing becomes unstable when the number of inputs per cell is below a threshold value, which is independent of network size. If the number of neurons in the simulated network is relatively small, the number of synaptic inputs to a cell may become small and may fall below the critical value for synchrony (which can be ~100 synaptic inputs or more; see Golomb and Hansel 2000). To compensate for the small network, one has to increase the connectivity probabilities to unrealistically high values. Since we obtained clear ING and PING oscillations with the connection probabilities from the literature (see METHODS), we did not modify the values for connectivity probability, since unrealistically high values might raise new questions about the proper values that should have been used in this study.

It is a long-standing question to what extent gamma oscillations in networks with coupled excitatory and inhibitory neurons are determined by the ING or PING mechanism or by mixtures of both, e.g., during spatial visual attention (Buia and Tiesinga 2006; Tiesinga and Sejnowski 2009). Our results show that for highly synchronous oscillations only one mechanism, the one with the higher frequency, determines the network oscillation frequency. This is because the higher-

frequency mechanism recruits the vast majority of available neurons in the network, such that the other mechanism cannot exist. In RESULTS we analyzed this behavior for networks with type I and type II interneurons, using both computer simulations for a network with many neurons (Figs. 6 and 7), as well as theoretical analyses for simple networks with two interacting neurons (Figs. 8 and 9).

While in both types of networks the dominating rhythm will be the one of ING or PING that generates the higher frequency, the results of our study also reveal a clear difference for the behavior of a network with coupled pyramidal cells and interneurons for type I and type II interneurons: For type I interneurons, the frequency of network oscillations will be slightly above the higher of the reduced-network ING and reduced-network PING oscillation frequencies, whereas for type II interneurons the frequencies of the network oscillation can be between the frequencies for reduced-network ING and reduced-network PING. Figure 6C, *left*, for the network with type I interneurons shows that for increasing drive to the interneurons, ING suppresses the PING-driven oscillation in the network and takes over for larger input values to the E cells (Fig. 6D). In both cases, the oscillation frequency smoothly increases. For a network with type II interneurons (Fig. 7, B and C, *left*) the transition is more complex, with a rapid transition from PING-driven oscillations to ING-driven oscillations (green line in Fig. 7B, *left*) or nonmonotonic changes of frequency (Fig. 7C, *left*). The more rapid transition from PING to ING in networks with type II interneurons is in agreement with results presented by Börgers and Walker (2013) for the suppression transition from PING to ING with suppressed E neurons. They find that the transition tends to be both narrower and more orderly for networks with type II interneurons than when the I cells are of type I.

Our results suggest possible approaches to experimentally distinguish between ING and PING oscillations with active E cells in *in vitro* studies. In the first approach, the external drive to the E cells should be kept constant while the external drive $I_{0,I}$ to I cells is varied. When the oscillations are dominated by PING, the rate of change in the frequency of the rhythm will increase when the external drive $I_{0,I}$ to the I cells increases (cf. Fig. 6C, *left*, and Fig. 7B, *left*). In contrast, the rate of change of the oscillation frequency decreases with increasing $I_{0,I}$ when the oscillations are dominated by ING. Note that the oscillation frequency itself increases in both cases with $I_{0,I}$, so an observation of frequency increase cannot be used to distinguish PING and ING. If the PING rhythm dominates the network dynamics and the interneurons are of type I, the frequency varies similarly with changes in $I_{0,E}$. In networks with type II interneurons, the nonmonotonic dependence near the ING-PING transition may be a characteristic hallmark to detect the oscillation character: Decrease of the frequency when increasing $I_{0,E}$ indicates ING; increase indicates PING. If the variation range of the driving current covers the transition region itself, it will be marked by a strong change in the E-cell firing frequency (cf. also Börgers and Walker 2013). Some experimental evidence is in line with these predictions. For example, Craig and McBain (2015) reported that optogenetic silencing of pyramidal cells in CA3, where the dominant form of gamma observed *in vitro* is PING, led to a significant increase in the peak frequency of the oscillation, as predicted by our results

(cf. the curves in Fig. 7C, *left*, at intermediate values of $I_{0,E}$). With the newly developed step-opsins (Prakash et al. 2012) one could selectively apply currents to neurons from specific populations over longer times. Thereby results as in Fig. 6, B–D, and Fig. 7, A–C, could be obtained experimentally. This will allow a test of our simulation results and predictions in this report, and it may reveal how ING and PING oscillations interact.

APPENDIX

In this appendix we give a summarized derivation of the oscillation frequency of the phase model described in RESULTS, with an excitatory and an inhibitory neuron. The text in this appendix is an extension of the description provided in METHODS.

Integrating Eq. 5 in the case of the iPRC given in Eq. 3 yields the transfer function for our sine neuron,

$$H_{\text{sine}}(\varphi; \Theta, \varepsilon) = \begin{cases} \frac{\Theta}{\pi} \arctan \left[\tan \left(\frac{\pi}{\Theta} \varphi \right) e^{-\frac{2\pi\varepsilon}{\Theta}} \right] & \text{for } \varphi \in \left(0, \frac{\Theta}{2} \right) \\ \frac{\Theta}{\pi} \arctan \left[\tan \left(\frac{\pi}{\Theta} \varphi \right) e^{-\frac{2\pi\varepsilon}{\Theta}} \right] + \Theta & \text{for } \varphi \in \left(\frac{\Theta}{2}, \Theta \right) \\ \varphi & \text{for } \varphi \in \left\{ 0, \frac{\Theta}{2}, \Theta \right\}. \end{cases} \quad (A1)$$

Since we are interested in the relative firing of the E and I neuron, the relevant variable is the relative phase $\Delta\varphi = \varphi_E - \varphi_I$ between the E and I neurons. We derive the transition from $\Delta\varphi$ to the phase difference $\Delta\tilde{\varphi}$ in the next cycle of firing. In particular, we derive an analytical expression for the firing frequency for the periodic state of the model, i.e., when $\Delta\tilde{\varphi}$ equals $\Delta\varphi$. We do so for three conditions for each of the two models: 1) for the dynamics of the interneuron without input from the E neuron (i.e., $\varepsilon_{E \rightarrow I} = 0$) (oscillations of the I neuron in this condition will henceforth be referred to as “pure” ING oscillations) and 2) for the dynamics of the E neuron with suprathreshold excitation of and feedback from an otherwise (nearly) silent interneuron. This condition is referred to as “pure” PING. The third condition refers to the dynamics of the full network.

The firing frequencies of the model for various conditions follow directly from the transfer functions (cf. Eq. 2 for the LIF neuron in METHODS and Eq. A1 for the sine neuron). For pure ING, the expression for the firing frequency of the interneuron is given by

$$f_{\text{LIF,ING}}(\tau, \Theta_I, \varepsilon_{I \rightarrow I}) = \left\{ \tau + \Theta_I + \ln \left[e^{-\tau} - \Gamma_{\text{LIF}}(\Theta_I, \varepsilon_{I \rightarrow I}) \right] \right\}^{-1} \quad (A2)$$

where Γ_{LIF} is defined in Eq. 2, for the LIF-LIF model (*model 1*) and

$$f_{\text{sine,ING}}(\tau, \Theta_I, \varepsilon_{I \rightarrow I}) = \left\{ \tau + \Theta_I - \frac{\Theta_I}{\pi} \arctan \left[\tan \left(\frac{\pi}{\Theta_I} \tau \right) e^{-\frac{2\pi\varepsilon_{I \rightarrow I}}{\Theta_I}} \right] \right\}^{-1} \quad (A3)$$

for the LIF-sine model (*model 2*).

When we refer to the network oscillations for pure PING and for the full network, we refer to periodic firing of the E neuron. For pure PING we assume a rather “ideal” rhythm with (effectively) suprathreshold excitation of the I neuron. We note that in the case of a LIF I neuron we can have real suprathreshold excitation: When the membrane potential exceeds the threshold, the neuron is reset immediately (second line in Eq. 2). In the case of a sine I neuron, the membrane potential can get arbitrarily near to the threshold in response to an input spike and can exceed it almost immediately after input due to external drive, such that we have effective suprathreshold

excitation. The firing frequency of the pure PING network (in particular of its E neuron) is given by

$$\begin{aligned} f_{\text{LIF},\text{PING}}(\tau, \Theta_E, \varepsilon_{I \rightarrow E}) \\ f_{\text{sine},\text{PING}}(\tau, \Theta_E, \varepsilon_{I \rightarrow E}) \end{aligned} = \left[2\tau + \Theta_E - H_{\text{LIF}}(2\tau; \Theta_E, \varepsilon_{I \rightarrow E}) \right]^{-1} = \left\{ 2\tau + \Theta_E + \ln [e^{-2\tau} - I_{\text{LIF}}(\Theta_E, \varepsilon_{I \rightarrow E})] \right\}^{-1} \quad (A4)$$

both for the LIF-LIF model (*model 1*) and the LIF-sine model (*model 2*). In this expression 2τ corresponds to the time delay of neuronal activity of the E neuron in the loop from the E to the I neuron and from the I neuron back to the E neuron. The term $H_{\text{LIF}}(2\tau; \Theta_E, \varepsilon_{I \rightarrow E})$ in Eq. A4 represents the transfer function of the E neuron (see Eq. 2) in response to the inhibition from the interneuron, which arrives at time 2τ after firing of the E neuron. The firing frequency only depends on the transfer function for the E neuron since the input to the I neuron is (practically) suprathreshold, which immediately initiates a spike in the I neuron.

In the full models, different modes of firing are possible for different parameter settings. Below we highlight those occurring for the parameter range covered by our figures.

For the LIF-LIF model, an ING rhythm occurs with frequency $f_{\text{LIF},\text{Full}}$ given by

$$f_{\text{LIF},\text{Full}}(\Delta\varphi) = \left[\tau + \Delta\varphi + \Theta_I - H_{\text{LIF}}(\tau + \Delta\varphi - \Delta\Theta; \Theta_E, \varepsilon_{I \rightarrow E}) \right]^{-1} \quad (A5)$$

where $\Delta\Theta$ is defined as $\Theta_E - \Theta_I$. The relevant phase difference $\Delta\varphi$ between the E and I neurons for a periodic ING rhythm in Eq. A5 is given by

$$\Delta\varphi = \ln \left(\frac{e^{-\tau} - e^{-H_{\text{LIF}}(\tau; \Theta_I, \varepsilon_{I \rightarrow I}) - \Delta\Theta} \pm \sqrt{[e^{-H_{\text{LIF}}(\tau; \Theta_I, \varepsilon_{I \rightarrow I}) - \Delta\Theta} - e^{-\tau}]^2 + 4e^{-\Delta\Theta} \Gamma(\Theta_E, \varepsilon_{I \rightarrow E}) \Gamma(\Theta_I, \varepsilon_{E \rightarrow I})}}{2e^{-\Delta\Theta} \Gamma(\Theta_E, \varepsilon_{I \rightarrow E})} \right). \quad (A6)$$

The rhythm with this relative phase $\Delta\varphi$ is found when $\Delta\Theta - \tau \leq \Delta\varphi < \Delta\Theta$. However, if the relative phase $\Delta\varphi$ is such that $\Delta\Theta \leq \Delta\varphi < \Delta\Theta + \tau$, we get another ING rhythm with frequency $f_{\text{LIF},\text{Full}}$ also given by Eq. A5, but the closed form of $\Delta\varphi$ is given by

$$\Delta\varphi = \ln \left(\frac{\Gamma(\Theta_I, \varepsilon_{I \rightarrow I}) + e^{-\tau + \Delta\Theta} - e^{-\tau}}{2\Gamma(\Theta_E, \varepsilon_{I \rightarrow E})} \pm \sqrt{[e^{-\tau} - \Gamma(\Theta_I, \varepsilon_{I \rightarrow I}) - e^{-\tau + \Delta\Theta}]^2 + 4\Gamma(\Theta_E, \varepsilon_{I \rightarrow E}) \Gamma(\Theta_I, \varepsilon_{E \rightarrow I}) e^{\Delta\Theta}} \right) \quad (A7)$$

Finally, for a PING rhythm where the excitatory input to the I neuron is suprathreshold, the firing frequency is described by $f_{\text{LIF},\text{PING}}$ (Eq. A4), with $\Delta\varphi$ given by

$$\Delta\varphi = \ln \left[\frac{e^{-\tau} - \Gamma(\Theta_I, \varepsilon_{I \rightarrow I})}{e^{-2\tau} - \Gamma(\Theta_E, \varepsilon_{I \rightarrow E})} \right] \quad (A8)$$

where $\Delta\varphi$ is in the range given by $\Delta\Theta + \tau \leq \Delta\varphi \leq \Theta_E + \tau - H_{\text{LIF}}(\Theta_I, \Theta_I, -\varepsilon_{E \rightarrow I})$.

For the LIF-sine model, the firing frequency $f_{\text{sine},\text{Full}}$ of the occurring ING rhythm is given by

$$f_{\text{sine},\text{Full}}(\Delta\varphi) = \left[\tau + \Delta\varphi + \Theta_I - H_{\text{LIF}}(\tau + \Delta\varphi - \Delta\Theta; \Theta_E, \varepsilon_{I \rightarrow E}) \right]^{-1} \quad (A9)$$

where $\Delta\varphi$ is a solution of the equation

$$0 = \Delta\varphi - H_{\text{LIF}}(\tau + \Delta\varphi - \Delta\Theta; \Theta_E, \varepsilon_{I \rightarrow E}) + H_{\text{sine}}[H_{\text{sine}}(\tau - \Delta\varphi + \Delta\Theta; \Theta_I, \varepsilon_{E \rightarrow I}) + \Delta\varphi - \Delta\Theta; \Theta_I, \varepsilon_{I \rightarrow I}] \quad (A10)$$

subject to the constraint $\Delta\Theta \leq \Delta\varphi < \Delta\Theta + \tau$. For the PING rhythm, the firing frequency of the LIF-sine model is given by

$$f_{\text{sine},\text{Full}}(\Delta\varphi) = \left[2\tau + \Theta_E + \Theta_I - H_{\text{sine}}(\Theta_E - \Delta\varphi + \tau; \Theta_I, \varepsilon_{E \rightarrow I}) - H_{\text{LIF}}(2\tau + \Theta_I - H_{\text{sine}}(\Theta_E - \Delta\varphi + \tau; \Theta_I, \varepsilon_{E \rightarrow I}); \Theta_E, \varepsilon_{I \rightarrow E}) \right]^{-1}, \quad (A11)$$

where $\Delta\varphi$ is a solution of the equation

$$0 = \Delta\varphi + H_{\text{sine}}(\tau; \Theta_I, \varepsilon_{I \rightarrow I}) - H_{\text{LIF}}[2\tau + \Theta_I - H_{\text{sine}}(\Theta_E - \Delta\varphi + \tau; \Theta_I, \varepsilon_{E \rightarrow I}); \Theta_E, \varepsilon_{I \rightarrow E}] \quad (A12)$$

and the phase difference $\Delta\varphi$ must satisfy $\Theta_E + \tau - H_{\text{sine}}(\Theta_I, \Theta_I, -\varepsilon_{E \rightarrow I}) < \Delta\varphi$ and $2\tau - \Delta\Theta \leq H_{\text{sine}}(\Theta_E - \Delta\varphi + \tau; \Theta_I, \varepsilon_{E \rightarrow I})$.

ACKNOWLEDGMENTS

We thank P. Tiesinga, F. Battaglia, and S. Jahnke for fruitful discussions.

GRANTS

This project was supported by the Netherlands Organization for Scientific Research (NWO 051.02.050), by the Max Kade Foundation New York, and by the German Federal Ministry of Education and Research (BMBF) through the Bernstein Network (Bernstein Award 2014).

DISCLOSURES

No conflicts of interest, financial or otherwise, are declared by the author(s).

AUTHOR CONTRIBUTIONS

A.V., R.-M.M., and S.G. conception and design of research; A.V. performed experiments; A.V. analyzed data; A.V., R.-M.M., and S.G. interpreted results of experiments; A.V. prepared figures; A.V., R.-M.M., and S.G. drafted manuscript; A.V., R.-M.M., and S.G. edited and revised manuscript; A.V., R.-M.M., and S.G. approved final version of manuscript.

REFERENCES

- Abbott LF, van Vreeswijk C.** Asynchronous states in networks of pulse-coupled oscillators. *Phys Rev E* 48: 1483–1490, 1993.
- Achuthan S, Canavier CC.** Phase-resetting curves determine synchronization, phase locking, and clustering in networks of neural oscillators. *J Neurosci* 29: 5218–5233, 2009.
- Ascoli GA, Atkeson JC.** Incorporating anatomically realistic cellular-level connectivity in neural network models of the rat hippocampus. *Biosystems* 79: 173–181, 2005.
- Bartos M, Vida I, Frotscher M, Geiger J, Jonas P.** Rapid signaling at inhibitory synapses in a dentate gyrus interneuron network. *J Neurosci* 21: 2687–2698, 2001.
- Bartos M, Vida I, Frotscher M, Meyer A, Monyer H, Geiger JR, Jonas P.** Fast synaptic inhibition promotes synchronized gamma oscillations in hippocampal interneuron networks. *Proc Natl Acad Sci USA* 99: 13222–13227, 2002.
- Bartos M, Vida I, Jonas P.** Synaptic mechanisms of synchronized gamma oscillations in inhibitory interneuron networks. *Nat Rev Neurosci* 8: 45–56, 2007.
- Bem T, Le Feuvre Y, Rinzel J, Meyrand P.** Electrical coupling induces bistability of rhythms in networks of inhibitory spiking neurons. *Eur J Neurosci* 22: 2661–2668, 2005.
- Bem T, Rinzel J.** Short duty cycle destabilizes a half-center oscillator, but gap junctions can restabilize the anti-phase pattern. *J Neurophysiol* 91: 693–703, 2004.
- Börgers C, Epstein S, Kopell NJ.** Background gamma rhythmicity and attention in cortical local circuits: a computational study. *Proc Natl Acad Sci USA* 102: 7002–7007, 2005.
- Börgers C, Kopell N.** Synchronization in networks of excitatory and inhibitory neurons with sparse, random connectivity. *Neural Comput* 15: 509–538, 2003.
- Börgers C, Kopell N.** Effects of noisy drive on rhythms in networks of excitatory and inhibitory neurons. *Neural Comput* 17: 557–608, 2005.
- Börgers C, Kopell NJ.** Gamma oscillations and stimulus selection. *Neural Comput* 20: 383–414, 2008.
- Börgers C, Krupa M, Gielen S.** The response of a classical Hodgkin-Huxley neuron to an inhibitory input pulse. *J Comput Neurosci* 28: 509–526, 2010.

- Börgers C, Walker B.** Toggling between gamma-frequency activity and suppression of cell assemblies. *Front Comput Neurosci* 7: 33, 2013.
- Bou-Flores C, Berger AJ.** Gap junctions and inhibitory synapses modulate inspiratory motoneuron synchronization. *J Neurophysiol* 85: 1543–1551, 2001.
- Bragin A, Jando G, Nádasdy Z, Hetke J, Wise K, Buzsáki G.** Gamma (40–100 Hz) oscillation in the hippocampus of the behaving rat. *J Neurosci* 15: 47–60, 1995.
- Brown E, Moehlis J, Holmes P.** On the phase reduction and response dynamics of neural oscillator populations. *Neural Comput* 16: 673–715, 2004.
- Brunel N.** Dynamics of sparsely connected networks of excitatory and inhibitory spiking neurons. *J Comput Neurosci* 8: 183–208, 2000.
- Brunel N, Hakim V.** Fast global oscillations in networks of integrate-and-fire neurons with low firing rates. *Neural Comput* 11: 1621–1671, 1999.
- Brunel N, Wang XJ.** What determines the frequency of fast network oscillations with irregular neural discharges? I. Synaptic dynamics and excitation-inhibition balance. *J Neurophysiol* 90: 415–430, 2003.
- Buia C, Tiesinga P.** Attentional modulation of firing rate and synchrony in a model cortical network. *J Comput Neurosci* 20: 247–264, 2006.
- Buzsáki G, Chrobak JJ.** Temporal structure in spatially organized neuronal ensembles: a role for interneuronal networks. *Curr Opin Neurobiol* 5: 504–510, 1995.
- Buzsáki G, Draguhn A.** Neuronal oscillations in cortical networks. *Science* 304: 1926–1929, 2004.
- Buzsáki G, Leung LW, Vanderwolf CH.** Cellular bases of hippocampal EEG in the behaving rat. *Brain Res* 287: 139–171, 1983.
- Buzsáki G, Wang XJ.** Mechanisms of gamma oscillations. *Annu Rev Neurosci* 35: 203–225, 2012.
- Canavier CC, Wang S, Chandrasekaran L.** Effect of phase response curve skew on synchronization with and without conduction delays. *Front Neural Circuits* 7: 194, 2013.
- Cardin JA, Carlen M, Meletis K, Knoblich U, Zhang F, Deisseroth K, Tsai LH, Moore CI.** Driving fast-spiking cells induces gamma rhythm and controls sensory responses. *Nature* 459: 663–667, 2009.
- Chow CC, Kopell N.** Dynamics of spiking neurons with electrical coupling. *Neural Comput* 12: 1643–1678, 2000.
- Chow CC, White JA, Ritt J, Kopell N.** Frequency control in synchronized networks of inhibitory neurons. *J Comput Neurosci* 5: 407–420, 1998.
- Cobb SR, Buhl EH, Halasy K, Paulsen O, Somogyi P.** Synchronization of neuronal activity in hippocampus by individual GABAergic interneurons. *Nature* 378: 75–78, 1995.
- Craig MT, McBain CJ.** Fast gamma oscillations are generated intrinsically in CA1 without the involvement of fast-spiking basket cells. *J Neurosci* 35: 3616–3624, 2015.
- Csicsvari J, Jamieson B, Wise KD, Buzsáki G.** Mechanisms of gamma oscillations in the hippocampus of the behaving rat. *Neuron* 37: 311–322, 2003.
- Cuturidis V, Graham B, Cobb S, Vida I.** *Hippocampal Microcircuits: A Computational Modeler's Resource Book*. New York: Springer, 2010.
- Deans MR, Gibson JR, Sellitto C, Connors BW, Paul DL.** Synchronous activity of inhibitory networks in neocortex requires electrical synapses containing connexin36. *Neuron* 31: 477–485, 2001.
- Debanne D, Guérineau NC, Gähwiler BH, Thompson SM.** Physiology and pharmacology of unitary synaptic connections between pairs of cells in areas CA3 and CA1 of rat hippocampal slice cultures. *J Neurophysiol* 73: 1282–1294, 1995.
- Di Garbo A, Barbi M, Chillemi S.** Synchronization in a network of fast-spiking interneurons. *Biosystems* 67: 45–53, 2002.
- Di Garbo A, Barbi M, Chillemi S.** The synchronization properties of a network of inhibitory interneurons depend on the biophysical model. *Biosystems* 88: 216–227, 2007a.
- Di Garbo A, Panarese A, Barbi M, Chillemi S.** The kinetics of the IPSC, the heterogeneity and the noise affect the firing coherence of a population of inhibitory interneurons. *Neurocomputing* 70: 2705–2715, 2007b.
- Economou MN, White JA.** Membrane properties and the balance between excitation and inhibition control gamma-frequency oscillations arising from feedback inhibition. *PLoS Comput Biol* 8: e1002354, 2012.
- Erisir A, Lau D, Rudy B, Leonard CS.** Function of specific K⁺ channels in sustained high-frequency firing of fast-spiking neocortical interneurons. *J Neurophysiol* 82: 2476–2489, 1999.
- Ermentrout B.** Type I membranes, phase resetting curves, and synchrony. *Neural Comput* 8: 979–1001, 1996.
- Ermentrout B, Pascal M, Gutkin B.** The effects of spike frequency adaptation and negative feedback on the synchronization of neural oscillators. *Neural Comput* 13: 1285–1310, 2001.
- Ernst U, Pawelzik K, Geisel T.** Synchronization induced by temporal delays in pulse-coupled oscillators. *Phys Rev Lett* 74: 1570–1573, 1995.
- Fisahn A, Contractor A, Traub R, Buhl E, Heinemann S, McBain C.** Distinct roles for the kainate receptor subunits GluR5 and GluR6 in kainate-induced hippocampal gamma oscillations. *J Neurosci* 24: 9658–9668, 2004.
- Fisahn A, Pike FG, Buhl EH, Paulsen O.** Cholinergic induction of network oscillations at 40 Hz in the hippocampus in vitro. *Nature* 394: 186–189, 1998.
- Forster E, Zhao ST, Frotscher M.** Laminating the hippocampus. *Nat Rev Neurosci* 7: 259–267, 2006.
- Fries P.** Neuronal gamma-band synchronization as a fundamental process in cortical computation. *Annu Rev Neurosci* 32: 209–224, 2009.
- Friesen WO.** Reciprocal inhibition: a mechanism underlying oscillatory animal movements. *Neurosci Biobehav Rev* 18: 547–553, 1994.
- Fukuda T, Kosaka T.** Gap junctions linking the dendritic network of GABAergic interneurons in the hippocampus. *J Neurosci* 20: 1519–1528, 2000.
- Galarreta M, Hestrin S.** A network of fast-spiking cells in the neocortex connected by electrical synapses. *Nature* 402: 72–75, 1999.
- Galarreta M, Hestrin S.** Electrical synapses between GABA-releasing interneurons. *Nat Rev Neurosci* 2: 425–433, 2001a.
- Galarreta M, Hestrin S.** Spike transmission and synchrony detection in networks of GABAergic interneurons. *Science* 292: 2295–2299, 2001b.
- Galarreta M, Hestrin S.** Electrical and chemical synapses among parvalbumin fast-spiking GABAergic interneurons in adult mouse neocortex. *Proc Natl Acad Sci USA* 99: 12438–12443, 2002.
- Geiger J, Lübbke J, Roth A, Frotscher M, Jonas P.** Submillisecond AMPA receptor-mediated signaling at a principal neuron-interneuron synapse. *Neuron* 18: 1009–1023, 1997.
- Gerstner W, Kistler WM.** *Spiking Neuron Models: Single Neurons, Populations, Plasticity*. Cambridge, UK: Cambridge Univ. Press, 2002.
- Gibson J, Beierlein M, Connors B.** Two networks of electrically coupled inhibitory neurons in neocortex. *Nature* 402: 75–79, 1999.
- Gibson JR, Beierlein M, Connors BW.** Functional properties of electrical synapses between inhibitory interneurons of neocortical layer 4. *J Neurophysiol* 93: 467–480, 2005.
- Gloveli T, Dugladze T, Saha S, Monyer H, Heinemann U, Traub R, Whittington M, Buhl E.** Differential involvement of oriens/pyramidal interneurons in hippocampal network oscillations in vitro. *J Physiol* 562: 131–147, 2005.
- Goel P, Ermentrout B.** Synchrony, stability, and firing patterns in pulse-coupled oscillators. *Physica D* 163: 191–216, 2002.
- Goldwyn J, Shea-Brown E.** The what and where of adding channel noise to the Hodgkin-Huxley equations. *PLoS Comput Biol* 7: e1002247, 2011.
- Golomb D, Hansel D.** The number of synaptic inputs and the synchrony of large, sparse neuronal networks. *Neural Comput* 12: 1095–1139, 2000.
- Gray CM.** Synchronous oscillations in neuronal systems: mechanisms and functions. *J Comput Neurosci* 1: 11–38, 1994.
- Gray CM, Singer W.** Stimulus-specific neuronal oscillations in orientation columns of cat visual cortex. *Proc Natl Acad Sci USA* 86: 1698–1702, 1989.
- Hajos N, Palhalimi J, Mann EO, Nemeth B, Paulsen O, Freund TF.** Spike timing of distinct types of GABAergic interneuron during hippocampal gamma oscillations in vitro. *J Neurosci* 24: 9127–9137, 2004.
- Hansel D, Mato G, Meunier C.** Synchrony in excitatory neural networks. *Neural Comput* 7: 307–337, 1995.
- Hopfield JJ.** Pattern-recognition computation using action-potential timing for stimulus representation. *Nature* 376: 33–36, 1995.
- Hormuzdi SG, Pais I, LeBeau FE, Towers SK, Rozov A, Buhl EH, Whittington MA, Monyer H.** Impaired electrical signaling disrupts gamma frequency oscillations in connexin 36-deficient mice. *Neuron* 31: 487–495, 2001.
- Izhikevich EM.** *Dynamical Systems in Neuroscience: The Geometry of Excitability and Bursting*. Cambridge, MA: MIT Press, 2007.
- Jeong HY, Gutkin B.** Study on the role of GABAergic synapses in synchronization. *Neurocomputing* 65: 859–868, 2005.
- Kilpatrick ZP, Ermentrout B.** Sparse gamma rhythms arising through clustering in adapting neuronal networks. *PLoS Comput Biol* 7: e1002281, 2011.
- Kopell N, Ermentrout B.** Chemical and electrical synapses perform complementary roles in the synchronization of interneuronal networks. *Proc Natl Acad Sci USA* 101: 15482–15487, 2004.

- Kopell N, LeMasson G.** Rhythmogenesis, amplitude modulation, and multiplexing in a cortical architecture. *Proc Natl Acad Sci USA* 91: 10586–10590, 1994.
- Krogh-Madsen T, Butera R, Ermentrout GB, Glass L.** Phase resetting neural oscillators: topological theory versus the real world. In: *Phase Response Curves in Neuroscience*, edited by Schultheiss NW, Prinz AA, Butera RJ. New York: Springer, 2012, p. 33–51.
- Krupa M, Gielen S, Gutkin B.** Adaptation and shunting inhibition leads to pyramidal/interneuron gamma with sparse firing of pyramidal cells. *J Comput Neurosci* 37: 357–376, 2014.
- Laurent G.** Olfactory network dynamics and the coding of multidimensional signals. *Nat Rev Neurosci* 3: 884–895, 2002.
- Lewis DA, Hashimoto T, Volk DW.** Cortical inhibitory neurons and schizophrenia. *Nat Rev Neurosci* 6: 312–324, 2005.
- Lewis TJ, Rinzel J.** Dynamics of spiking neurons connected by both inhibitory and electrical coupling. *J Comput Neurosci* 14: 283–309, 2003.
- Lisman JE.** Relating hippocampal circuitry to function: recall of memory sequences by reciprocal dentate-CA3 interactions. *Neuron* 22: 233–242, 1999.
- Lisman JE, Idiart MA.** Storage of 7 ± 2 short-term memories in oscillatory subcycles. *Science* 267: 1512–1515, 1995.
- Llinás RR, Ribary U, Jeanmonod D, Kronberg E, Mitra PP.** Thalamocortical dysrhythmia: a neurological and neuropsychiatric syndrome characterized by magnetoencephalography. *Proc Natl Acad Sci USA* 96: 15222–15227, 1999.
- Long MA, Deans MR, Paul DL, Connors BW.** Rhythmicity without synchrony in the electrically uncoupled inferior olive. *J Neurosci* 22: 10898–10905, 2002.
- Lyttton WW, Sejnowski TJ.** Simulations of cortical pyramidal neurons synchronized by inhibitory interneurons. *J Neurophysiol* 66: 1059–1079, 1991.
- Mann EO, Radcliffe CA, Paulsen O.** Hippocampal gamma-frequency oscillations: from interneurons to pyramidal cells, and back. *J Physiol* 562: 55–63, 2005.
- Mann-Metzer P, Yarom Y.** Electrotone coupling interacts with intrinsic properties to generate synchronized activity in cerebellar networks of inhibitory interneurons. *J Neurosci* 19: 3298–3306, 1999.
- McBain CJ, Fisahn A.** Interneurons unbound. *Nat Rev Neurosci* 2: 11–23, 2001.
- Memmesheimer RM.** Quantitative prediction of intermittent high-frequency oscillations in neural networks with supralinear dendritic interactions. *Proc Natl Acad Sci USA* 107: 11092–11097, 2010.
- Merriam EB, Netoff TI, Banks MI.** Bistable network behavior of layer I interneurons in auditory cortex. *J Neurosci* 25: 6175–6186, 2005.
- Meyrand P, Cattaert D, Ostaszewski H, Bem T.** Inhibitory network of spiking neurons may express a sharp peak of synchrony at low frequency band. *Biol Cybern* 101: 325–338, 2009.
- Nomura M, Aoyagi T.** Stability of synchronous solutions in weakly coupled neuron networks. *Prog Theor Phys* 113: 911–925, 2005.
- Nomura M, Fukai T, Aoyagi T.** Synchrony of fast-spiking interneurons interconnected by GABAergic and electrical synapses. *Neural Comput* 15: 2179–2198, 2003.
- Nowacki J, Osinga HM, Brown JT, Randall AD, Tsaneva-Atanasova K.** A unified model of CA1/3 pyramidal cells: an investigation into excitability. *Prog Biophys Mol Biol* 105: 34–48, 2011.
- Oh M, Matveev V.** Loss of phase-locking in non-weakly coupled inhibitory networks of type-I model neurons. *J Comput Neurosci* 26: 303–320, 2009.
- Palhalmi J, Paulsen O, Freund TF, Hajos N.** Distinct properties of carbachol- and DHPG-induced network oscillations in hippocampal slices. *Neuropharmacology* 47: 381–389, 2004.
- Pfeuty B, Mato G, Golomb D, Hansel D.** Electrical synapses and synchrony: the role of intrinsic currents. *J Neurosci* 23: 6280–6294, 2003.
- Pfeuty B, Mato G, Golomb D, Hansel D.** The combined effects of inhibitory and electrical synapses in synchrony. *Neural Comput* 17: 633–670, 2005.
- Prakash R, Yizhar O, Grewe B, Ramakrishnan C, Wang N, Goshen I, Packer AM, Peterka DS, Yuste R, Schnitzer MJ, Deisseroth K.** Two-photon optogenetic toolbox for fast inhibition, excitation and bistable modulation. *Nat Methods* 9: 1171–1179, 2012.
- Routh BN, Johnston D, Harris K, Chitwood RA.** Anatomical and electrophysiological comparison of CA1 pyramidal neurons of the rat and mouse. *J Neurophysiol* 102: 2288–2302, 2009.
- Schoffelen JM, Oostenveld R, Fries P.** Neuronal coherence as a mechanism of effective corticospinal interaction. *Science* 308: 111–113, 2005.
- Sohal V, Zhang F, Yizhar O, Deisseroth K.** Parvalbumin neurons and gamma rhythms enhance cortical circuit performance. *Nature* 459: 698–702, 2009.
- Spencer KM, Nestor PG, Niznikiewicz MA, Salisbury DF, Shenton ME, McCarley RW.** Abnormal neural synchrony in schizophrenia. *J Neurosci* 23: 7407–7411, 2003.
- Tamas G, Buhl EH, Lorincz A, Somogyi P.** Proximally targeted GABAergic synapses and gap junctions synchronize cortical interneurons. *Nat Neurosci* 3: 366–371, 2000.
- Tateno T, Harsch A, Robinson HP.** Threshold firing frequency-current relationships of neurons in rat somatosensory cortex: type 1 and type 2 dynamics. *J Neurophysiol* 92: 2283–2294, 2004.
- Tateno T, Robinson HP.** Phase resetting curves and oscillatory stability in interneurons of rat somatosensory cortex. *Biophys J* 92: 683–695, 2007.
- Terman D, Kopell N, Bose A.** Dynamics of two mutually coupled slow inhibitory neurons. *Physica D* 117: 241–275, 1998.
- Terman D, Lee E, Rinzel J, Bem T.** Stability of anti-phase and in-phase locking by electrical coupling but not fast inhibition alone. *SIAM J Appl Dyn Syst* 10: 1127–1153, 2011.
- Tiesinga P, Sejnowski TJ.** Cortical enlightenment: are attentional gamma oscillations driven by ING or PING? *Neuron* 63: 727–732, 2009.
- Tiesinga PH, Fellous JM, Jose JV, Sejnowski TJ.** Computational model of carbachol-induced delta, theta, and gamma oscillations in the hippocampus. *Hippocampus* 11: 251–274, 2001.
- Tiesinga PH, Fellous JM, Sejnowski TJ.** Spike-time reliability of periodically driven integrate-and-fire neurons. *Neurocomputing* 44: 195–200, 2002.
- Tikidji-Hamburyan RA, Martinez JJ, White JA, Canavier CC.** Resonant interneurons can increase robustness of gamma oscillations. *J Neurosci* 35: 15682–15695, 2015.
- Traub R, Whittington M, Colling S, Buzsáki G, Jefferys J.** Analysis of gamma rhythms in the rat hippocampus in vitro and in vivo. *J Physiol* 493: 471–484, 1996.
- Traub RD, Draguhn A, Whittington MA, Baldeweg T, Bibbig A, Buhl EH, Schmitz D.** Axonal gap junctions between principal neurons: a novel source of network oscillations, and perhaps epileptogenesis. *Rev Neurosci* 13: 1–30, 2002.
- Traub RD, Kopell N, Bibbig A, Buhl EH, LeBeau FE, Whittington MA.** Gap junctions between interneuron dendrites can enhance synchrony of gamma oscillations in distributed networks. *J Neurosci* 21: 9478–9486, 2001.
- Uhlhaas PJ, Singer W.** Neural synchrony in brain disorders: relevance for cognitive dysfunctions and pathophysiology. *Neuron* 52: 155–168, 2006.
- van Vreeswijk C, Abbott LF, Ermentrout GB.** When inhibition not excitation synchronizes neural firing. *J Comput Neurosci* 1: 313–321, 1994.
- Wang XJ, Buzsáki G.** Gamma oscillation by synaptic inhibition in a hippocampal interneuronal network model. *J Neurosci* 16: 6402–6413, 1996.
- Wang XJ, Rinzel J.** Alternating and synchronous rhythms in reciprocally inhibitory model neurons. *Neural Comput* 4: 84–97, 1992.
- Welch PD.** The use of fast Fourier transform for the estimation of power spectra: a method based on time averaging over short, modified periodograms. *IEEE Trans Acoust* 15: 70–73, 1967.
- White JA, Chow CC, Ritt J, Soto-Trevino C, Kopell N.** Synchronization and oscillatory dynamics in heterogeneous, mutually inhibited neurons. *J Comput Neurosci* 5: 5–16, 1998a.
- White JA, Klink R, Alonso A, Kay AR.** Noise from voltage-gated ion channels may influence neuronal dynamics in the entorhinal cortex. *J Neurophysiol* 80: 262–269, 1998b.
- Whittington M, Cunningham M, LeBeau F, Racca C, Traub R.** Multiple origins of the cortical γ rhythm. *Dev Neurobiol* 71: 92–106, 2011.
- Whittington MA, Traub RD, Jefferys JG.** Synchronized oscillation in interneuron networks driven by metabotropic glutamate receptor activation. *Nature* 373: 612–615, 1995.
- Whittington MA, Traub RD, Kopell N, Ermentrout B, Buhl EH.** Inhibition-based rhythms: experimental and mathematical observations on network dynamics. *Int J Psychophysiol* 38: 315–336, 2000.
- Winfree AT.** Biological rhythms and behavior of populations of coupled oscillators. *J Theor Biol* 16: 15–42, 1967.